

CENPD-390-NP

# **The Advanced PHOENIX and POLCA Codes for Nuclear Design of Boiling Water Reactors**

**ABB Combustion Engineering Nuclear Power**



LEGAL NOTICE

THIS REPORT WAS PREPARED AS AN ACCOUNT OF WORK SPONSORED BY ABB COMBUSTION ENGINEERING NUCLEAR POWER, INC. NEITHER ABB COMBUSTION ENGINEERING NUCLEAR POWER, INC. NOR ANY PERSON ACTING ON ITS BEHALF:

A. MAKES ANY WARRANTY OR REPRESENTATION, EXPRESS OR IMPLIED INCLUDING THE WARRANTIES OF FITNESS FOR A PARTICULAR PURPOSE OR MERCHANTABILITY, WITH RESPECT TO THE ACCURACY, COMPLETENESS, OR USEFULNESS OF THE INFORMATION CONTAINED IN THIS REPORT, OR THAT THE USE OF ANY INFORMATION, APPARATUS, METHOD, OR PROCESS DISCLOSED IN THIS REPORT MAY NOT INFRINGE PRIVATELY OWNED RIGHTS; OR

B. ASSUMES ANY LIABILITIES WITH RESPECT TO THE USE OF, OR FOR DAMAGES RESULTING FROM THE USE OF, ANY INFORMATION, APPARATUS, METHOD OR PROCESS DISCLOSED IN THIS REPORT.

**CENPD-390-NP**

**The Advanced PHOENIX and POLCA Codes for  
Nuclear Design of Boiling Water Reactors**

**December 1999**

**ABB Combustion Engineering Nuclear Power, Inc.**

Copyright 1999, Combustion Engineering, Inc.  
All rights reserved



**TABLE OF CONTENTS**

**1.0 INTRODUCTION ..... 1**

1.1 PURPOSE OF THE REPORT ..... 1

1.2 BACKGROUND ..... 2

1.3 APPLICABILITY OF THE REPORT ..... 5

1.4 ORGANIZATION OF THE REPORT ..... 5

**2.0 PHOENIX..... 9**

2.1 OVERVIEW OF PHOENIX..... 9

2.2 PHOENIX CROSS SECTION LIBRARY ..... 9

    2.2.1 Processing of ENDF/B-VI Data ..... 9

    2.2.2 Resonance Region Treatment ..... 10

    2.2.3 Thermal Region Treatment ..... 10

    2.2.4 Data Adjustment ..... 10

2.3 DEPLETION CALCULATIONS ..... 11

**3.0 QUALIFICATION OF THE NEW LIBRARY WITH PHOENIX ..... 13**

3.1 REACTIVITY COMPARISONS FOR PIN CELL CRITICALS ..... 13

    3.1.1 Experiment Description ..... 13

    3.1.2 Modeling Considerations ..... 14

    3.1.3 Results ..... 14

3.2 REACTIVITY COMPARISONS FOR TRX AND BAPL CRITICALS ..... 14

    3.2.1 Experiment Description ..... 15

    3.2.2 Modeling Considerations ..... 15

    3.2.3 Results ..... 15

3.3 NONUNIFORM KRITZ BA-75 CRITICAL EXPERIMENTS ..... 15

    3.3.1 Experiment Description ..... 16

    3.3.2 Modeling Conditions ..... 16

    3.3.3 Results ..... 17

3.4 NONUNIFORM KRITZ PU CRITICAL EXPERIMENTS ..... 18

    3.4.1 Experiment Description ..... 18

    3.4.2 Modeling Conditions ..... 19

    3.4.3 Results ..... 19

3.5 CONCLUSIONS ..... 20

**4.0 POLCA ..... 30**

4.1 OVERVIEW OF POLCA ..... 30

    4.1.1 General Features ..... 31

4.2 CALCULATIONAL FLOW ..... 32

4.3 NEUTRONICS MODEL ..... 32

4.4 CROSS SECTION MODEL ..... 33

4.5 BWR THERMAL-HYDRAULICS MODEL ..... 35

4.6 DETECTOR MODEL ..... 39

4.7 ALBEDO MODEL ..... 40

4.8 XENON TRANSIENT MODEL ..... 40

4.9 PIN POWER RECONSTRUCTION MODEL ..... 41

    4.9.1 Radial Shape Function ..... 42

    4.9.2 Control Rod History and the Radial Shape Function ..... 42

4.10 AXIAL HOMOGENIZATION ..... 43

4.11 DEPLETION CALCULATIONS ..... 44



4.11.1 Nuclide Concentration Tracking .....	44
4.11.2 Detector Depletion.....	46
4.12 POWER PEAKING FACTORS AND THERMAL MARGINS .....	46
4.12.1 Power Peaking Factors and Distributions .....	47
4.12.2 Fission Heat Load Calculations .....	47
4.12.3 Critical Power Ratio.....	49
4.12.4 Pellet-Clad Interaction.....	49
5.1 NEUTRONIC MODEL VERIFICATION .....	52
5.1.1 IAEA Benchmark .....	52
5.1.2 BIBLIS Benchmark .....	53
5.1.3 DVP Benchmark .....	54
5.1.4 Intra-Nodal Depletion Benchmark .....	55
5.2 THERMAL-HYDRAULICS MODEL VERIFICATION .....	56
5.2.1 Pressure Drop Comparisons.....	57
5.2.2 Assembly Flow Rate Comparisons.....	58
5.3 PIN POWER CALCULATIONAL CAPABILITY QUALIFICATION .....	59
5.3.1 NEACRP-L336 Benchmark .....	59
5.3.2 Fuel Rod Gamma Scans.....	61
5.4 CORE REACTIVITY AND POWER DISTRIBUTIONS .....	65
5.4.1 POLCA Reactivity Predictions .....	67
5.4.2 POLCA Comparisons with TIP Measurements .....	68
5.4.3 Nodal Gamma Scans.....	70
5.5 PERFORMANCE RELATIVE TO CURRENT PHOENIX/POLCA SYSTEM .....	75
5.5.1 Reactivity Comparisons .....	75
5.5.2 TIP Comparisons.....	76
<b>6.0 SUMMARY .....</b>	<b>81</b>
6.1 PHOENIX BENCHMARKS TO TEST THE NEW LIBRARY.....	81
6.2 POLCA QUALIFICATION.....	82
6.2.1 Reactivity.....	83
6.2.2 Power Distributions.....	83
6.2.3 Pressure Drops and Relative Assembly Flow.....	85
6.3 OVERALL CONCLUSION.....	86
<b>7.0 REFERENCES .....</b>	<b>87</b>
<b>APPENDIX A [PROPRIETARY INFORMATION DELETED] .....</b>	<b>A-1</b>
<b>APPENDIX B [PROPRIETARY INFORMATION DELETED] .....</b>	<b>B-1</b>
<b>APPENDIX C [PROPRIETARY INFORMATION DELETED] .....</b>	<b>C-1</b>
<b>APPENDIX D [PROPRIETARY INFORMATION DELETED] .....</b>	<b>D-1</b>

## 1.0 INTRODUCTION

The two principal computer programs for Boiling Water Reactor steady-state nuclear design and analysis used by ABB are PHOENIX and POLCA. The PHOENIX code is a two-dimensional multi-group transport theory code used to calculate the lattice physics constants of BWR fuel assemblies. The POLCA code is a two-group nodal code used for the three-dimensional simulation of the nuclear and thermal-hydraulic conditions in BWR cores. In addition, several auxiliary codes are also utilized in order to facilitate calculations and transfer of data between the aforementioned codes.

This report provides a detailed description of the verification that has been performed to qualify the computer codes and analysis methods which are used for the nuclear design and analysis of Boiling Water Reactors. Included are substantial improvements to the POLCA computer code. This report will be referenced in future license submittals utilizing the PHOENIX/POLCA system.

### 1.1 PURPOSE OF THE REPORT

The purpose of this topical report is to present the qualification work that has been performed for a new version of the PHOENIX/POLCA code system. PHOENIX and POLCA are the lattice physics and three-dimensional core simulator codes used by ABB for BWR nuclear design and analyses. The qualification results establish the accuracy and uncertainties associated with the PHOENIX/POLCA system. Since the calculational models, approximations and methods in the PHOENIX code are the same as those described in Reference 1, NRC review of the PHOENIX calculational methods is not required and the calculational model descriptions are not repeated in this report. Qualification results with the new 34-group cross section library are provided as an illustration of the ABB methodology for qualifying a new cross section library. PHOENIX, and the associated nuclear data pre- and post-processing codes, has been modified only to the extent required to support the new cross section library and the POLCA improvements. For the POLCA code, improvements have been made to the calculational methods that warrant NRC review and acceptance for referencing in licensing applications.

## 1.2 BACKGROUND

The PHOENIX and POLCA codes were originally submitted for review in licensing topical reports (References 2 and 3) by Westinghouse Electric Corp. The nuclear methods used by ABB Atom (formerly ASEA Atom) in Sweden were described in the topical reports.

These reports were reviewed and accepted by the U.S. NRC in References 4 and 5. In 1988, ABB Atom continued the licensing of the ABB BWR reload methodology initiated by Westinghouse. The transfer of the licensing effort from Westinghouse to ABB was formally facilitated by ABB resubmitting NRC approved licensing topical reports under the ABB ownership. The NRC acknowledged the transfer of approval in Reference 6. Reference 1 is the licensing topical report describing the nuclear design and analysis programs resubmitted by ABB. As a result of the acquisition of Combustion Engineering, Inc. by the parent company of ABB Atom, the U.S. operations of ABB Atom were consolidated within Combustion Engineering, Inc. (Reference 7). The ABB Combustion Engineering Nuclear Power Division of Combustion Engineering, Inc. is the cognizant organization for BWR reload fuel application in the United States. Quality control, maintenance, and implementation for the complete ABB U.S. reload fuel licensing methodologies resides with ABB Combustion Engineering Nuclear Power.

The ABB BWR nuclear design system of codes is presented in Figure 1.1, which outlines the relationship between the individual computer codes. PHOENIX and POLCA are considered the two major codes in the system, whereas the other codes shown in the figure perform various auxiliary functions.

The calculational models, approximations and methods in the PHOENIX code are the same as those described in Reference 1. Therefore, NRC review of the PHOENIX calculational methods is not required and the calculational model descriptions are not repeated in this report. The only differences between the PHOENIX versions are the use of a new cross section library and a modified PHOENIX output cross section data base. The modifications to the PHOENIX output data base were required due to the improved methods in POLCA.

As opposed to PHOENIX, the POLCA calculational models have been substantially improved. These improvements include:

1. An enhanced cross section treatment based on microscopic and macroscopic cross sections to accurately accommodate the impact of various effects including those due to control rods and spacer grids. The spectral history is specifically accounted for by solving depletion chains for heavy nuclides and fission products. This treatment allows a substantially more accurate treatment of spectral and burnup effects than the treatment previously presented in Reference 1.
2. The new POLCA version utilizes a full two-group diffusion theory model rather than the modified one-group model described in Reference 1. The use of discontinuity factors and burnup dependent spatial cross section variation provides accurate nodal power distributions and a firm basis for pin power reconstruction.
3. The new POLCA version has the capability of utilizing pin power reconstruction to accommodate the effect of neutron leakage from adjacent assemblies on pin powers.
4. The new POLCA version contains a more detailed hydraulic model relative to that described in Reference 1. This improved model allows for axial flow area changes as well as part length rods.

In conjunction with the introduction of the improved version of POLCA, ABB is adopting a new cross section library based on ENDF/B-VI (Reference 8) in place of the previous library based on ENDF/B-IV. It is introduced with the new version of POLCA since the ABB methodology for adopting a new cross section library requires extensive benchmark testing against higher order methods, lattice data, and plant operating data. Therefore, the benchmarking requirements of the new POLCA version and the new library overlap. As a result, the comparisons of POLCA predictions with measurement data are based on the new library. Comparisons of PHOENIX predictions with two-dimensional measurement data are also provided as an illustration of the ABB methodology for the introduction of a new library.

As noted in Figure 1.1, several auxiliary codes are used in conjunction with PHOENIX and POLCA. To manipulate cross section library data, preparation codes FOBUS, HEBE and PHULCAN are used. FOBUS was originally described in Reference 1, and the description in Reference 1 continues to be valid. A new preprocessor to PHOENIX, IFIGEN, was

developed to aid in the generation of cross section data bases. For transferring cross section data from PHOENIX to POLCA, codes CoreLink and TABBE are used.

FOBUS is a Monte Carlo program used to generate burnable absorber cross section tables to be used by PHOENIX. This program performs a detailed flux calculation in (R,Z) geometry for the central pin in a 3x3 array. A very fine mesh can be used for the flux calculation with up to 15 radial zones and 13 axial segments used to model the distribution of compositions in the absorber pin (total of up to 195 regions). The results from FOBUS can be passed on to HEBE or incorporated directly into the PHOENIX library.

HEBE is the service program for the PHOENIX cross section library. It supports the more detailed structure of the 34-group library relative to the one described in Reference 1. It lets the user perform such tasks as creating a new library, listing data, adding burnable absorber data, and other similar tasks.

PHULCAN reads definitions of burnup chains for isotopes included in the library and constructs depletion chain data in a format suitable for PHOENIX.

The task of preparing PHOENIX input has been simplified by the development of IFIGEN, a preprocessor that generates PHOENIX input files for branch calculations to aid in the process of generating cross section data bases required by the POLCA cross section model.

The data processing code PHIPO, originally described in Reference 1, has been replaced by CoreLink. CoreLink has the same functions as PHIPO but with extended output data capabilities, accommodating the more detailed cross section model of POLCA. CoreLink is a data handling and post-processing code which prepares cell data for POLCA from data files generated by the PHOENIX (or other) lattice physics code. CoreLink processes the data for a single fuel segment type at a time and produces cell data tables with a prescribed ASCII format and structure.

The program TABBE reads the ASCII tables produced by CoreLink and stores them in binary format in a so called cell data file. TABBE may also be employed to generate ASCII tables from the binary cell data file.

### 1.3 APPLICABILITY OF THE REPORT

The intended scope of the PHOENIX/POLCA computational methods include the following BWR nuclear design and analysis applications:

- Power distribution calculations
- Thermal-hydraulic calculations
- Fuel management calculations
- Control rod worth and shutdown margin calculations
- Generation of control rod pattern sequences
- Thermal margin evaluations
- Reactivity coefficients and kinetics parameters
- In-core detector simulation
- Core reactivity calculations
- Generation of process computer constants
- Generation of power to flow control lines
- Simulation of normal operation power maneuvers including load follow
- Evaluation of anticipated operational occurrences and accidents which can be treated with steady-state methods
- Input to dynamic transient and accident analyses

The intended scope of use for the PHOENIX/POLCA code system includes all design related steady-state calculations required for the nuclear design and licensing analysis of Boiling Water Reactors.

### 1.4 ORGANIZATION OF THE REPORT

Chapter 2 summarizes the basic cross section library and depletion calculations used in the PHOENIX code. PHOENIX is used for generation of few-group microscopic and macroscopic, cell and assembly average cross sections needed as input to POLCA. As previously mentioned, the calculational models, approximations and methods of PHOENIX are the same as previously reviewed by the NRC (Reference 1). The calculational model descriptions are not repeated in detail in this report.

Chapter 3 contains the verification demonstrating that PHOENIX, in conjunction with the new cross section library, performs its specified tasks. This verification consists of comparisons with local power distributions from multiple critical experiments. Reactivity data from uniform and nonuniform critical experiments are used to demonstrate that the PHOENIX cross section library performs accurately together with the models for constructing multi-group average microscopic cross sections and for computing the neutron flux distributions within pin cells of the BWR geometry.

Chapter 4 includes the calculational flow, methods and approximations in the POLCA code. POLCA is used for the three-dimensional simulation of the nuclear and thermal-hydraulic conditions in BWR cores. The multiple neutronic and thermal-hydraulic models implemented in POLCA are described in some detail.

Chapter 5 provides verification of POLCA's models in the form of comparisons with numerical benchmarks. It also contains qualification of the PHOENIX/POLCA code system in the form of comparisons with gamma scan measurements and flow measurements, as well as core reactivity and TIP readings for four benchmark reactors. The chapter concludes by presenting reactivity and TIP reading comparisons between the improved PHOENIX/POLCA code system described in this report and the previous system presented in Reference 1.

Chapter 6 provides a summary.

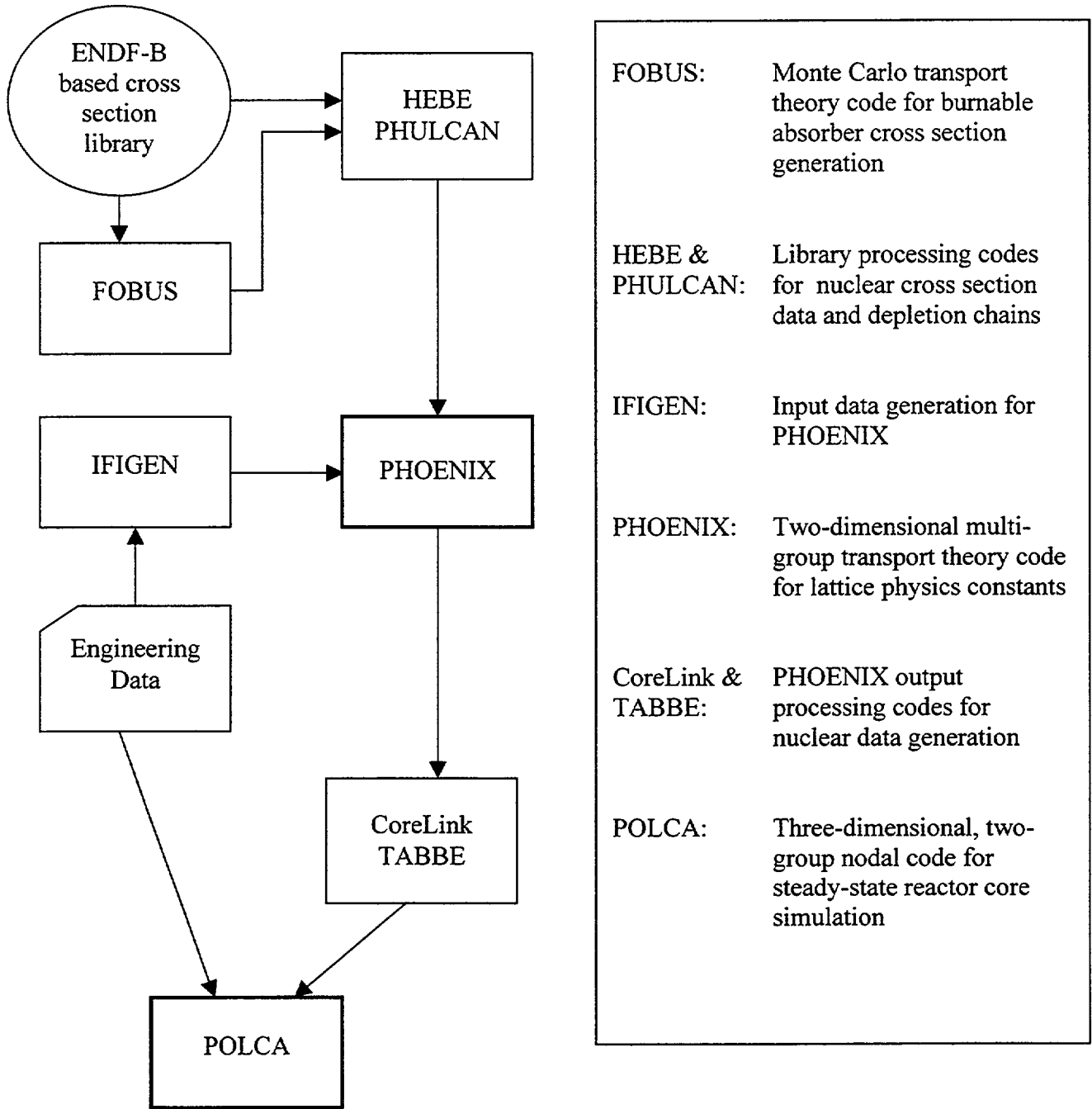


Figure 1.1: ABB Code System for BWR Nuclear Design and Analysis

*This Page Intentionally Left Blank*

## 2.0 PHOENIX

### 2.1 OVERVIEW OF PHOENIX

The PHOENIX code was previously described for BWR use in Reference 1. The only change in PHOENIX which significantly affects numerical results relative to the description in Reference 1 is the introduction of a new cross section library based on the evaluated nuclear data file, ENDF/B-VI. This chapter includes a description of the new ENDF/B-VI based cross section library.

### 2.2 PHOENIX CROSS SECTION LIBRARY

The new BWR cross section libraries based on ENDF/B-VI for use with PHOENIX employ 34 and 89 neutron energy groups. They contain multi-group microscopic neutron cross sections, fission spectra, fission product yields, energy yields, and other supplemental data. It is ABB's intention to use the 34-group library for design, core follow and licensing analyses.

The qualification of the PHOENIX/POLCA system described in this report is based on this new 34-group library. Also available for use with PHOENIX is an 89-group library which has been used for verifying the group structure of the 34-group library. For both libraries, the source of the basic cross section data is ENDF/B-VI, Releases 1, 2 and 3 (Reference 8).

#### 2.2.1 Processing of ENDF/B-VI Data

The processing code NJOY 91, with updates through 105 (Reference 9) and extended as described below, was used for processing the ENDF/B-VI data. A master library was initially created (Reference 10). This was an "Application Independent" (as defined in Reference 11) library with 190 neutron energy groups. The master library was then used for condensation to all other libraries such as the 34-group and 89-group libraries. The group structures of the 34-group and 89-group libraries are shown in Tables 2.1 and 2.2. Table 2.3 lists characteristics of the 34-group library.

The NJOY capabilities were augmented by an extended version of RABBLE. The original version of RABBLE (Reference 12) calculated point cross sections from the Single Level Breit-Wigner (SLBW) formula. In the extended version used, RABBLE worked as a module of NJOY and was capable of reading the continuous cross section data from the PENDF point files of NJOY. This permitted use of more accurate models than the SLBW and a very fine energy mesh in a cylindrical pin.

Appendix A lists all the materials (MAT) such as isotopes, natural elements, mixtures, burnable absorbers and special materials in the 34-group library. The material identifiers (MAT ID) shown are the identifiers used by PHOENIX. Several burnable absorbers are included which were generated with FOBUS for multiple  $Gd_2O_3$  concentrations and pellet dimensions. The table also shows which materials include resonance tables (RES TABLES) in the library, and which materials only contain absorption cross sections (ABS XS ONLY).

### 2.2.2 Resonance Region Treatment

Resolved resonances generally fit in the interval 1.855 eV to 9.119 keV, and in this region capture and fission cross sections are in the form of resonance tables. The content of these two-dimensional tables is computed by RABBLE. They are tabulated parametrically in temperature and in equivalent potential scattering via an equivalence theorem. PHOENIX then uses the same equivalence theorem to retrieve and interpolate between values in the table.

### 2.2.3 Thermal Region Treatment

The ENDF/B-VI files are processed with the THERMR module of NJOY to provide cross sections and scattering matrices in the thermal energy region (0 eV - 3.928 eV). In this region, upscattering is modeled. The cross sections of isotopes containing resonances in the thermal region are Doppler broadened. Scattering matrices are tabulated as a function of temperature, spanning the range of power reactor operation and with sufficient detail to permit linear interpolation.

### 2.2.4 Data Adjustment

Although ENDF/B-VI, Rev. 3 includes many features improving basic cross section accuracy, U-238 resonance capture still remained in need of improvement (References 10 and 13). Therefore, based on the analyses described in References 10 and 13, **[PROPRIETARY INFORMATION DELETED]**.

## 2.3 DEPLETION CALCULATIONS

Examples of the depletion chains for fission products, heavy elements and for burnable absorbers are shown in Appendices B, C, and D, respectively. These chains may be modified from time to time as new data become available. Any modifications affecting numerical values will be internally documented as part of the process of establishing, validating and documenting the corresponding modified biases and uncertainties.

The method for solving the various chains is similar to the method that was documented in Reference 1. **[PROPRIETARY INFORMATION DELETED]**.

**Tables 2.1 through 2.3**

**[PROPRIETARY INFORMATION DELETED]**

### 3.0 QUALIFICATION OF THE NEW LIBRARY WITH PHOENIX

The primary application of PHOENIX is to generate the few-group nodal cross sections and other physics constants for POLCA. Therefore, the benchmarking of POLCA to plant data described in Chapter 5 provides the best overall qualification of PHOENIX. However, PHOENIX predictions based on the new 34-group library have also been directly compared to measured data as presented in this chapter.

Comparisons with uniform lattice critical measurements test PHOENIX's ability to accurately calculate reactivity over a wide range of lattice parameters. Because of the simple geometry in those experiments, the comparisons primarily provide verification and validation of the new cross section library.

In addition, the ability of PHOENIX to accurately predict bundle reactivity and internal (local) power distributions has been verified using experiments on nonuniform lattices performed at the KRITZ critical facility.

#### 3.1 REACTIVITY COMPARISONS FOR PIN CELL CRITICALS

The objective of this benchmark is to verify the new cross section library by showing PHOENIX's reactivity prediction capability over a wide range of uniform lattice criticals. The 101 criticals (Reference 14), referred to as the "Strawbridge & Barry Criticals," cover a wide range of lattice parameters, bounding the normal design application for which PHOENIX is intended to be used, and providing a severe test of PHOENIX's ability to accurately predict reactivities over a broad range of conditions.

##### 3.1.1 Experiment Description

The experiments in this set were all uniform pin cells; 74 out of the 101 cases were hexagonal cells and the remaining 27 were square cells. Both uranium dioxide ( $\text{UO}_2$ ) and metallic uranium, with different enrichments of U-235, were used as the fuel material. Light water ( $\text{H}_2\text{O}$ ) at room temperature was used as the moderator in all experiments.

Table 3.1 shows that the range of conditions in this experimental data base is extensive and spans the range of modern LWRs.

### 3.1.2 Modeling Considerations

Except for the hexagonal cases, the PHOENIX models developed resembled the same conditions as the experimental cases. Since PHOENIX can not model hexagonal lattices, those cases were approximated as square geometries which preserve material region volumes.

Several of the analyzed experiments had relatively large water/fuel volume ratios. For those cases, a more detailed mesh structure in the moderator region was used.

### 3.1.3 Results

Table 3.2 shows the average  $k_{\text{effective}}$  and corresponding standard error of the mean value ( $S/\sqrt{N}$ ) for several subgroups of the 101 experiments analyzed. Those results were obtained from PHOENIX using the 34-group library. Table 3.3 shows similar results obtained with the 89-group library. Table 3.4 includes experimental parameters and results (using the 34-group library) for each of the 101 critical experiments.

The results of the reactivity calculations for the 101 pin cell criticals show that PHOENIX agrees well with experiment. Not only is the overall average  $k_{\text{effective}}$  of **[PROPRIETARY INFORMATION DELETED]** satisfactory, but individual category averages are also acceptable. It should also be noted that the mean  $k_{\text{effective}}$  and standard errors for the 34-group and 89-group results are in good agreement. This shows that the new 34-group, ENDF/B-VI based library performs well.

As indicated in Reference 14, the calculated standard errors are not strictly calculational uncertainties or due to code errors. Considerable contributions come from such effects as uncertainties in the experimental bucklings, neglect of fuel, clad and moderator impurities, and uncertainties in the dimensions, pellet densities and enrichments.

## 3.2 REACTIVITY COMPARISONS FOR TRX AND BAPL CRITICALS

As for the previous set of experiments, the objective of this benchmark is to verify the new PHOENIX cross section library in terms of calculated reactivities. The five experiments in this group involved uniform lattices. These criticals are widely used for thermal data testing by the "Cross Section Evaluation Working Group" (CSEWG).

### 3.2.1 Experiment Description

The TRX-1 and TRX-2 experiments were water moderated lattices of slightly enriched (1.3% U-235) metallic uranium rods with a diameter of 0.9830 cm arranged in a triangular lattice. The BAPL-1, BAPL-2 and BAPL-3 experiments were also water moderated lattices in a triangular lattice, but contain uranium oxide rods (1.311% U-235 enrichment) with a diameter of 0.9728 cm. The experiments are further described in Reference 15.

### 3.2.2 Modeling Considerations

As was mentioned previously, PHOENIX can not explicitly model hexagonal lattices. For this reason, an equivalent square lattice was used which preserved moderator volume. Also, as for the Strawbridge & Barry experiments, the TRX and BAPL experiments were analyzed with an adequate number of radial meshes in the moderator region.

### 3.2.3 Results

Table 3.5 presents the PHOENIX results for the five experiments analyzed. For these cases, PHOENIX was used with the 34-group library. The table shows that the BAPL reactivity levels (average  $k_{\text{effective}}$  of [PROPRIETARY INFORMATION DELETED]) are consistent with the Strawbridge & Barry average for the UO<sub>2</sub> subgroup (average  $k_{\text{effective}}$  of [PROPRIETARY INFORMATION DELETED]). This again shows good performance for the 34-group library.

However, there appears to be a bias in the TRX cases (average  $k_{\text{effective}}$  of [PROPRIETARY INFORMATION DELETED]) relative to the Strawbridge & Barry metal lattice subset (average  $k_{\text{effective}}$  of [PROPRIETARY INFORMATION DELETED]). This may be due to [PROPRIETARY INFORMATION DELETED].

## 3.3 NONUNIFORM KRITZ BA-75 CRITICAL EXPERIMENTS

During 1968-1975, an extensive series of critical experiments were performed in the KRITZ reactor at Studsvik in Sweden. The KRITZ reactor was designed to perform critical experiments with full size fuel assemblies at temperatures up to 245°C. Additional details about these experiments are found in Reference 16.

### 3.3.1 Experiment Description

As shown in Figure 3.1, experiments using 4x4 assembly arrays with different inter-assembly gap configurations were compared with corresponding PHOENIX predictions. These 4x4 assembly cores were contained in a square vessel. The distance from the inner vessel to the first fuel assembly was 12 cm in the south and west directions and 20 cm in the north and east directions. As noted in Table 3.6, eight cases were analyzed using the upper configuration shown in Figure 3.1, while four cases were performed using the lower configuration. For all cases, the wide gap between assemblies was 1.986 cm, while the narrow gap was 1.036 cm.

Each of the 16 assemblies contained 8x8 fuel pins. The corner pins (3 in each corner) had slightly smaller diameters than normal pins and also different lattice pitches. In some of the cases, the central four assemblies contained pins with  $Gd_2O_3$  burnable absorbers. The average enrichment of the fuel assemblies was 2.64 wt% U-235. The burnable absorbers pins contained fuel with a uniform  $Gd_2O_3$  concentration of 1.98 wt%. In some cases, a stainless steel boron carbide control rod was placed between the four central assemblies. Soluble boron and moderator height were used as the control mechanism.

The recorded measurements were the boron concentration, moderator temperature, and axial buckling (obtained from the water height and extrapolated length determined from measured axial flux distributions) at the critical condition. Relative fission rates for selected pins were also recorded.

### 3.3.2 Modeling Conditions

PHOENIX has the capability to treat four assemblies together in a 2x2 array (quadruple assembly option) with reflective boundary conditions. This option was used to model one quarter of the KRITZ core. Specifically, the southwest quadrant of the core was modeled with a reflector half-thickness of 20 cm along the southern and western faces. This provided 40 cm of moderator gap to the next assembly in the infinite array produced by the reflective boundary condition. This distance was considered sufficient to eliminate interference of the mirrored part. The effect of the vessel sides was not considered. The two-dimensional calculations were performed at the experimental moderator temperature and boron concentration as well as the measured axial buckling.

### 3.3.3 Results

Table 3.6 presents the experimental conditions, measurements and PHOENIX calculated results for each of the twelve cases analyzed. The critical boron concentration, experimental temperature, critical buckling (defined by the water height), water density and calculated  $k_{\text{effective}}$  (with PHOENIX) are presented in Table 3.6.

The average  $k_{\text{effective}}$  for the twelve configurations analyzed is [PROPRIETARY INFORMATION DELETED] with a standard deviation of [PROPRIETARY INFORMATION DELETED]. These results are consistent with the Strawbridge & Barry and the BAPL experiments previously discussed.

The  $k_{\text{effective}}$  values for configurations with burnable absorbers are well predicted. Rodded cases are also well predicted. Comparing controlled cases with corresponding uncontrolled cases (2:2 vs. 2:1, 2:4 vs. 2:3), a difference of roughly [PROPRIETARY INFORMATION DELETED] pcm was calculated. This implies a [PROPRIETARY INFORMATION DELETED] of control rod worth, which is considered acceptable.

For cases 2:3, 3:1 and 3:2, measurements were performed both at high and low moderator temperatures. This allows the computation of the isothermal coefficient (ITC) for those cases. The ITC can be obtained by assuming that any soluble boron calculation error is negligible and comparing  $k_{\text{effective}}$  values at high and low temperatures for the three pairs of measurements. Table 3.7 shows the computed ITCs.

Although the calculated temperature coefficient is nonzero, the average value of [PROPRIETARY INFORMATION DELETED] represents a major improvement in calculational accuracy relative to calculations performed with earlier cross section libraries. Results using previous libraries have been on the order of -2 pcm/°C. This progress is due to improvements in U-235 thermal cross sections provided by the ENDF/B-VI data (Reference 10).

Figures 3.2 through 3.5 show the comparisons between the measured and calculated fission rate distributions, which have been normalized to the averaged fission rate density of all measured pins for each experiment. They correspond to case 2:1 at 23.5°C, case 2:3 (with BA) at 243.2°C, case 3:1 at 242.3°C and case 3:2 (with BA) at 241.9°C, respectively.

The agreement between measurement and calculated fission rates is excellent with an average deviation of [PROPRIETARY INFORMATION DELETED]. The experimental uncertainty is claimed to be in the order of 1 to 2%. The maximum difference observed was only [PROPRIETARY INFORMATION DELETED].

### 3.4 NONUNIFORM KRITZ PU CRITICAL EXPERIMENTS

Critical experiments using mixed oxide fuel rods with 1.50% PuO<sub>2</sub> were performed in 1972-73 in the pressurized KRITZ critical facility in Studsvik, Sweden. These experiments are similar to those described in Section 3.3.

#### 3.4.1 Experiment Description

The reactor description is the same as for the set of KRITZ experiments described in Section 3.3. The only difference is that the distance from the square vessel to the first fuel assembly was modified to 7.9 cm on the south and west sides.

The cores were arranged in the same way as for the KRITZ BA-75 experiments. Each configuration was a square array of 16 fuel assemblies. The assemblies consisted of three different types of 8x8 fuel pins:

BWR-70 64 UO<sub>2</sub> pins,  
Pu-Island 45 UO<sub>2</sub> pins + 19 PuO<sub>2</sub>/UO<sub>2</sub> pins,  
Pu-Max 8 UO<sub>2</sub> pins + 56 PuO<sub>2</sub>/UO<sub>2</sub> pins.

The UO<sub>2</sub> pins were enriched to 1.86 wt% U-235. The PuO<sub>2</sub>/UO<sub>2</sub> pins were 0.16 wt% U-235/U and 1.50 wt% PuO<sub>2</sub>/UO<sub>2</sub>. Figure 3.6 shows the KRITZ core arrangements for these experiments, and Figure 3.7 shows the three types of fuel assemblies.

As for the previous KRITZ experiments discussed in Section 3.3, the recorded measurements were the boron concentration, moderator temperature, and axial buckling (water height) at the critical condition. Relative fission rates for selected pins were also recorded.

### 3.4.2 Modeling Conditions

The modeling conditions for the KRITZ PU experiments described in this section are essentially the same as for the KRITZ BA-75 experiments described in Section 3.3.

### 3.4.3 Results

Table 3.8 presents the experimental conditions, measurements and calculated PHOENIX results for each of the eight cases analyzed. The critical boron concentration, experimental temperature, critical buckling (defined by the water height), water density and  $k_{\text{effective}}$  calculated by PHOENIX are presented in Table 3.8.

The average  $k_{\text{effective}}$  for the eight configurations analyzed is [PROPRIETARY INFORMATION DELETED] with a standard deviation of [PROPRIETARY INFORMATION DELETED]. No significant difference appears to exist between  $\text{PuO}_2$  and  $\text{UO}_2$  cases. This absence of a criticality bias between  $\text{PuO}_2$  and  $\text{UO}_2$  cases is presumably a result of the improved Pu cross section data in ENDF/B-VI. The results are consistent with the Strawbridge & Barry, BAPL and the KRITZ BA-75 cases previously discussed.

The ITCs are computed for two KRITZ PU configurations as was done for the KRITZ BA-75 cases. Table 3.9 shows the computed ITCs. The resulting isothermal temperature coefficient [PROPRIETARY INFORMATION DELETED], which is considered to be acceptable.

Figures 3.8 and 3.9 show the comparison between measured and calculated fission rate distributions for case 1:1 at 241.1°C and case 1:4 at 239.2°C, respectively (for case 1:4, only pins in the central assembly (2,3) were measured.) The results were normalized to the averaged fission rate density of all measured pins for each experiment.

The agreement between measured fission rate distributions and calculated values is excellent with a mean absolute deviation of [PROPRIETARY INFORMATION DELETED], and a maximum difference of [PROPRIETARY INFORMATION DELETED]. As for the KRITZ BA-75 experiments, the experimental uncertainty for these experiments is claimed to be in the order of 1 to 2%.

### 3.5 CONCLUSIONS

The experimental conditions covered by these benchmark demonstrate the reliability of PHOENIX and its new 34-group library over a broad range of conditions. It should be reiterated that the range of experimental conditions frequently exceed the normal range for BWR applications.

Table 3.10 provides a summary of the benchmark critical experiment results in this chapter. The relatively high standard deviation observed for the Strawbridge & Barry set seen in Table 3.10 is attributed to the relatively broad range of conditions and the use of measured data from a wide range of sources. The standard deviation in Table 3.10 of **[PROPRIETARY INFORMATION DELETED]** is not markedly different from that found by Strawbridge & Barry in 1965 while the category means and overall means are significantly different. This indicates that experimental errors may be larger than the errors in modern methods.

The conclusions from each group of comparisons may be summarized as follows:

1. The calculated reactivity level for the overall collection of Strawbridge & Barry criticals (101 cases) and for the various subgroups is in excellent agreement with the measurements (see Table 3.2).
2. The three BAPL cases are the most relevant for LWR application. Both the reactivity level and standard deviation are excellent (see Table 3.5).
3. The KRITZ experiments provide good reactivity benchmarks for the combination of PHOENIX and the new cross section library. These cases were complex core geometries with homogeneous and inhomogeneous fuel designs as well as variations in U and Pu and burnable absorber content.

The 12 cases in the KRITZ BA-75 series reflect the capability of PHOENIX and the new cross section library to accurately treat reactivity, burnable absorber worth, control rod worth, and relative pin power. They also demonstrate a relatively low reactivity dependence on moderator temperature. Reactivity level is predicted with the same excellent consistency as for the Strawbridge & Barry and BAPL cases (see Table 3.6). Standard deviations are low and consistent with the BAPL experiments. Control rod worths and burnable absorber worths are well predicted. The isothermal coefficient calculation performance is

markedly improved with the new cross section library relative to older libraries (see Table 3.7).

The KRITZ PU series (8 cases) reflect the capability of PHOENIX and the new cross section library to accurately treat reactivity level and relative pin power in  $\text{PuO}_2$  lattices (see Table 3.8). Statistical tests show that the predicted mean  $\text{PuO}_2$   $k_{\text{effective}}$  values and corresponding standard deviations are not significantly different than the corresponding values for  $\text{UO}_2$  lattices. This consistency of PHOENIX's predictive capability for  $\text{UO}_2$  and  $\text{PuO}_2$  experiments represents a significant improvement which is attributed to the new ENDF/B-VI based library. The results confirm the reliability of PHOENIX in the presence of high Pu concentrations and for high inter-assembly leakage.

In overall conclusion, these benchmark calculations reflect the capability of PHOENIX with the new ENDF/B-VI based cross section library to accurately predict reactivity level with very low deviations as well as accurately predict relative pin power (fission rate) distributions. Isothermal temperature coefficient performance, as well as predicted control rod worths and burnable absorber worths, have improved relative to older cross section libraries. The combination of these results confirm that PHOENIX, in conjunction with the new ENDF/B-VI based 34-group library, provides state-of-the-art reactivity and relative pin power predictions for a broad range of conditions and temperatures.

**Table 3.1: Parameter Ranges for Pin Cell Criticals**

	Experiment	Typical Modern LWR Fuel
Water / U ratio	1.00 - 11.94	2.0 - 5.0*
Lattice pitch (cm)	0.95 - 4.95	1.20 - 1.63
Pellet diameter (cm)	0.44 - 2.35	0.78 - 1.04
Clad outer diam (cm)	0.44 - 2.35	0.95 - 1.25
Enrichment (wt%)	1.04 - 4.07	0.71 - 5.00
Boron content (ppm)	0 - 3392	0 - 3000

\* Void and gaps in BWR fuel considered

**Table 3.2: Pin Cell Criticals Results (34-Group Library)**

Experiment Group	Number of Data Points	Average $k_{\text{effective}}$	Standard Error of Mean Value (pcm)
Hexagonal Lattice	74	[Proprietary Information Deleted]	[Proprietary Information Deleted]
Square Lattice	27	[Proprietary Information Deleted]	[Proprietary Information Deleted]
Aluminum Clad	56	[Proprietary Information Deleted]	[Proprietary Information Deleted]
Stainless Steel Clad	25	[Proprietary Information Deleted]	[Proprietary Information Deleted]
Dissolved Boron	7	[Proprietary Information Deleted]	[Proprietary Information Deleted]
No Boron	94	[Proprietary Information Deleted]	[Proprietary Information Deleted]
UO <sub>2</sub> Experiments	40	[Proprietary Information Deleted]	[Proprietary Information Deleted]
Uranium Metal Experiments	61	[Proprietary Information Deleted]	[Proprietary Information Deleted]
All Data	101	[Proprietary Information Deleted]	[Proprietary Information Deleted]

**Table 3.3: Pin Cell Criticals Results (89-Group Library)**

Experiment Group	Number of Data Points	Average $k_{\text{effective}}$	Standard Error of Mean Value (pcm)
Hexagonal Lattice	74	[Proprietary Information Deleted]	[Proprietary Information Deleted]
Square Lattice	27	[Proprietary Information Deleted]	[Proprietary Information Deleted]
Aluminum Clad	56	[Proprietary Information Deleted]	[Proprietary Information Deleted]
Stainless Steel Clad	25	[Proprietary Information Deleted]	[Proprietary Information Deleted]
Dissolved Boron	7	[Proprietary Information Deleted]	[Proprietary Information Deleted]
No Boron	94	[Proprietary Information Deleted]	[Proprietary Information Deleted]
UO <sub>2</sub> Experiments	40	[Proprietary Information Deleted]	[Proprietary Information Deleted]
Uranium Metal Experiments	61	[Proprietary Information Deleted]	[Proprietary Information Deleted]
All Data	101	[Proprietary Information Deleted]	[Proprietary Information Deleted]

**Table 3.4 [Proprietary Information Deleted]**

**Table 3.5: TRX and BAPL Experiments Results**

Experiment	$k_{\text{effective}}$
TRX-1	[Proprietary Information Deleted]
TRX-2	[Proprietary Information Deleted]
BAPL-1	[Proprietary Information Deleted]
BAPL-2	[Proprietary Information Deleted]
BAPL-3	[Proprietary Information Deleted]

**Table 3.6: KRITZ BA-75 Experiments Results**

Core No.	Boron Conc.(ppm)	Temp (C)	Buckling ( $m^{-2}$ )	Water ( $g/cm^3$ )	Control Blade	BA pins*	Calc. $k_{\text{effective}}$
2:1	304.6	23.5	7.942	0.9975	no	0	[Proprietary Information Deleted]
	364.5	24.2	3.454	0.9973	no	0	[Proprietary Information Deleted]
2:2	33.5	22.4	7.555	0.9977	yes	0	[Proprietary Information Deleted]
	78.7	23.5	3.895	0.9975	yes	0	[Proprietary Information Deleted]
2:3	266.2	23.5	3.979	0.9975	no	2	[Proprietary Information Deleted]
	247.4	243.2	3.634	0.8091	no	2	[Proprietary Information Deleted]
2:4	33.5	22.5	3.186	0.9975	yes	2	[Proprietary Information Deleted]
2:5	52.8	20.6	3.103	0.9982	no	7	[Proprietary Information Deleted]
3:1	306.2	22.5	5.580	0.9975	no	0	[Proprietary Information Deleted]
	366.2	242.3	2.866	0.8103	no	0	[Proprietary Information Deleted]
3:2	31.9	18.9	8.317	0.9985	no	5	[Proprietary Information Deleted]
	63.5	241.9	2.810	0.8109	no	5	[Proprietary Information Deleted]

\* Number of BA pins in each of the four central assemblies

**Table 3.7: Isothermal Coefficient for KRITZ BA-75 Experiments**

Case	Delta T (°C)	Delta k (pcm)	ITC (pcm/°C)
2:3	219.7	[Proprietary Information Deleted]	[Proprietary Information Deleted]
3:1	219.8	[Proprietary Information Deleted]	[Proprietary Information Deleted]
3:2	223.0	[Proprietary Information Deleted]	[Proprietary Information Deleted]
Average ITC			[Proprietary Information Deleted]

**Table 3.8: KRITZ PU Experiments Results**

Core No.	Boron Conc.(ppm)	Temp (C)	Buckling (m <sup>-2</sup> )	Water (g/cm <sup>3</sup> )	Calc. k <sub>effective</sub>
1:1	44.7	22.8	7.590	0.9977	[Proprietary Information Deleted]
	48.3	241.1	4.200	0.8122	[Proprietary Information Deleted]
1:2	61.9	18.6	7.080	0.9985	[Proprietary Information Deleted]
	61.9	88.4	7.610	0.9662	[Proprietary Information Deleted]
1:4	40.7	22.9	10.290	0.9976	[Proprietary Information Deleted]
	44.3	239.2	7.310	0.8150	[Proprietary Information Deleted]
1:5	40.7	22.4	11.510	0.9977	[Proprietary Information Deleted]
	56.1	88.4	11.060	0.9662	[Proprietary Information Deleted]

**Table 3.9: Isothermal Coefficient for KRITZ PU Experiments**

Case	Delta T (°C)	Delta k (pcm)	ITC (pcm/°C)
1:1	218.3	[Proprietary Information Deleted]	[Proprietary Information Deleted]
1:4	216.3	[Proprietary Information Deleted]	[Proprietary Information Deleted]
Average ITC			[Proprietary Information Deleted]

**Table 3.10: Summary of Benchmark Critical Experiments**

Experiment Set	No. of Experiments	k <sub>effective</sub>	Std Dev (pcm)
Strawbridge & Barry (UO <sub>2</sub> only)	40	[Proprietary Information Deleted]	[Proprietary Information Deleted]
BAPL	3	[Proprietary Information Deleted]	[Proprietary Information Deleted]
KRITZ BA-75	12	[Proprietary Information Deleted]	[Proprietary Information Deleted]
KRITZ PU	8	[Proprietary Information Deleted]	[Proprietary Information Deleted]
Pooled Data	63	[Proprietary Information Deleted]	[Proprietary Information Deleted]

(1,4)	(2,4)	(3,4)	(4,4)
(1,3)	(2,3)	(3,3)	(4,3)
(1,2)	(2,2)	(3,2)	(4,2)
(1,1)	(2,1)	(3,1)	(4,1)

For cases 2:1, 2:2, 2:3, 2:4 and 2:5

(1,4)	(2,4)	(3,4)	(4,4)
(1,3)	(2,3)	(3,3)	(4,3)
(1,2)	(2,2)	(3,2)	(4,2)
(1,1)	(2,1)	(3,1)	(4,1)

For cases 3:1 and 3:2

Figure 3.1: KRITZ BA-75 Core Configurations with Assembly Coordinates

**Figures 3.2 through 3.5**

**[PROPRIETARY INFORMATION DELETED]**

BWR-70



Pu-Island



Pu-Max

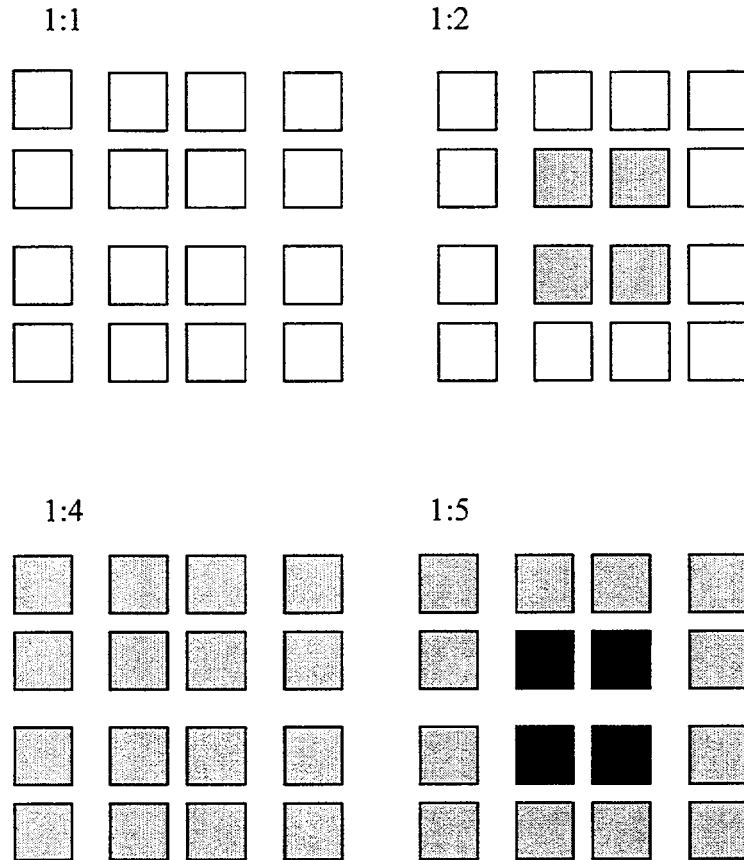


Figure 3.6: KRITZ PU Experiments Core Configurations

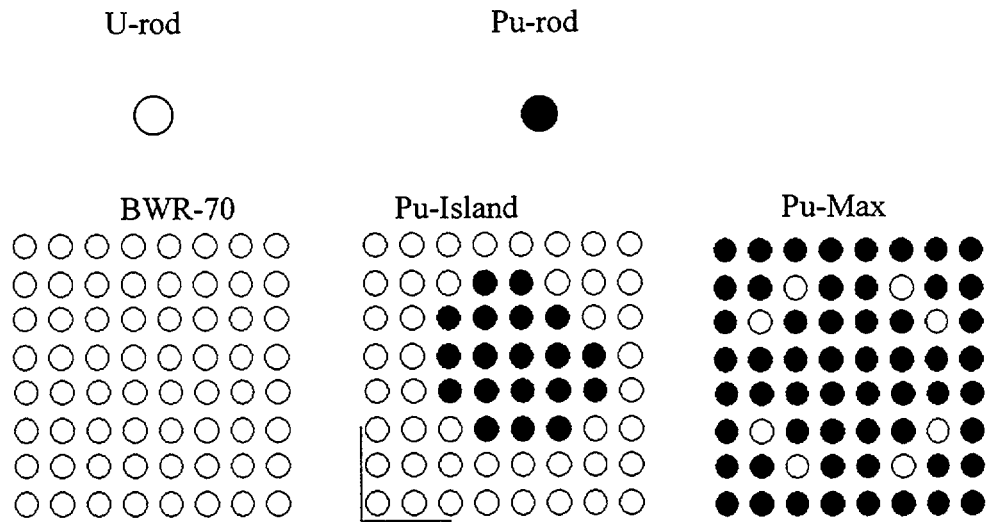


Figure 3.7: KRITZ PU Experiments Fuel Pin Configurations

**Figures 3.8 through 3.9**

**[PROPRIETARY INFORMATION DELETED]**

## 4.0 POLCA

### 4.1 OVERVIEW OF POLCA

POLCA is a three-dimensional code for simulating the neutronic, thermal, and hydraulic behavior of a reactor core. The code solves the coupled thermal-hydraulic and neutronic equations. The version described in this report is used for steady-state design and licensing applications as well as for anticipated operational occurrences (AOOs) and accident analyses which can be treated with steady-state methods. The PHOENIX/POLCA system is also used to prepare input for and initialize dynamic AOOs and accident analyses.

POLCA solves the two-group diffusion equation employing an analytic nodal method. The code calculates the three-dimensional power distribution in the reactor taking into account all important phenomena that must be included. In POLCA, the reactor core is divided into computational nodes in which the neutronic characteristics of each node are described by homogenized equivalent two-group macroscopic cross sections. The three-dimensional power distribution calculated by POLCA includes the thermal-hydraulic feedback effects of the coolant flow and void distribution, the influence of control rods, as well as important reactivity feedback effects such as those due to Doppler feedback and xenon absorption. POLCA can model either quarter-core, half-core, or full core geometries.

The BWR thermal-hydraulics (T-H) models in POLCA treat the lower plenum, each fuel assembly, a lumped inter-assembly bypass channel, the upper plenum, steam separators, steam dome, downcomer, and main recirculating pumps. POLCA provides the capability to describe the hydraulic characteristics of the core region in detail. Separate loss coefficients can be provided for important assembly components such as inlet orifices, bottom nozzles, tie plates and spacers. Geometric axial variations in the fuel assemblies and specific leakage paths to bypasses can be described. The impact of void content on the calculated axial power distribution within the fuel assemblies is supported by an empirical void correlation. Using fuel assembly internal rod power distributions in conjunction with nodal powers, linear heat generation rates and critical power ratios can be determined. The average planar linear heat generation rate is also evaluated for each fuel assembly node. The T-H module can handle reactor pressures from 1 to 200 bar and a temperature range from room temperature to hot full power. The T-H module can be executed as a free-standing entity or as part of an integrated power/void iteration in the POLCA analysis.

The formulation of POLCA described in this chapter provides accurate representations of parameters important for design and licensing applications. These parameters include thermal margins, feedback mechanisms, fuel burnup, xenon distributions, simulation of the signals from the in-core detectors (TIP and LPRM), and the calculation of the reactivity margins at shutdown conditions.

#### 4.1.1 General Features

POLCA is the main working tool for in-core fuel management activities as well as analysis of Anticipated Operational Occurrences (AOOs) and accidents which can be treated with steady-state methods, and the initialization of AOOs and accidents described by time-dependent methods. Examples of applications of POLCA are

- Bundle design
- Core reload design
- AOOs and accidents which can be analyzed with steady-state methods
- Control rod sequence design
- Reactivity coefficient calculations
- Fuel depletion
- Control rod depletion
- Traversing in-core probes (TIP) analysis
- Load swing planning and analysis
- Power ascension and descension between cold conditions and hot full power
- Power or coolant flow control planning
- Boration using the standby liquid control system
- Cold critical calculations
- Safeguards: fissile material inventory
- On-line core monitoring
- Core operation optimization

POLCA solves the coupled neutronic and thermal-hydraulic problem with state-of-the-art methods providing a high degree of spatial resolution. The three-dimensional core power distribution can be computed to the local level within each assembly. Distributions of all important parameters required for design and actual licensing applications can also be computed. All core states from cold, xenon free to hot full power are covered.

The geometric flexibility of POLCA includes three main features:

A. Core radial symmetry may be chosen with:

- No symmetry
- Half core mirror or rotational symmetry
- Quarter core mirror or rotational symmetry

B. The core may be surrounded by a layer of reflector material [PROPRIETARY INFORMATION DELETED].

C. The computational unit cell used in POLCA's three-dimensional calculations is a segment of a fuel bundle. Hereafter it is referred to as a "node". The axial nodalization may be chosen freely without requirements of equal node heights. The axial mesh structures for detectors and control rods can be chosen independently of the computational mesh used for solving the neutron diffusion equation. Likewise the axial material description of fuel assemblies is independent of the computational mesh. These features allow more accurate modeling of the fuel assembly and reactor core than the previous version of POLCA described in Reference 1.

## 4.2 CALCULATIONAL FLOW

The structure of POLCA is summarized in Figure 4.1. The code consists of four main parts: input, power/void iteration loop, post-processing, and output. The input and output parts are self explanatory and will not be discussed further. Most of the calculations are performed in the remaining two parts. The thermal-hydraulics and neutronic equations are solved in the power/void iteration loop. Pin power reconstruction and thermal margin calculations are performed during post-processing. Discussion of methods and equations used in those two parts of the code are presented throughout this chapter.

## 4.3 NEUTRONICS MODEL

POLCA solves the two-group diffusion equation employing a method similar to that referred to as the Analytic Nodal Method (ANM) in Reference 17. The method takes the three-dimensional diffusion equation and converts it into three one-dimensional equations, with one equation for each spatial direction. Those equations are coupled through the neutron leakage from one direction to another, referred to as transverse leakages, and explained further in Reference 18. The shape of each transverse leakage is estimated by fitting a parabola to the known average leakages of

three adjacent nodes. The analytical solution to the inhomogeneous one-dimensional diffusion equation is used to derive a relationship between node surface net currents and node average fluxes. This relationship is then substituted into the node balance equation to eliminate net currents as unknowns to yield an equation which is similar to that resulting from the finite difference approximation. Thus, a very efficient algorithm for solving the diffusion equation is derived with, formally, only one unknown per node.

In addition to the use of transverse leakages for spatial decoupling, the second main feature of POLCA's nodal method is a spectral analysis method used to compute the analytic matrix functions which appear in the nodal coupling relations. This spectral analysis approach has been used independently in Reference 19.

Modern homogenization principles are also accounted for in the nodal equations through the use of discontinuity factors to describe flux continuity conditions at nodal interfaces. In addition, smooth intra-nodal variations of cross sections are allowed to account for burnup induced heterogeneities. These advanced methods are capable of yielding an accuracy of two percent or better in node powers (see Section 5.1).

The neutronic computational module produces node average fluxes and node interface average fluxes and net currents. The flux variation inside the node is calculated by the pin power reconstruction approach summarized in Section 4.9.

#### 4.4 CROSS SECTION MODEL

The cross section model in POLCA includes a subset of the nuclides in the PHOENIX 34-group library. The choice of nuclides is discussed in Section 4.11. The function of the cross section module of POLCA is to produce:

- Macroscopic two-group, node average cross sections ( $D_1, D_2, \Sigma_r, \Sigma_{a1}, \Sigma_{a2}, \nu\Sigma_{f1}, \nu\Sigma_{f2}$ )
- Microscopic two-group, node average cross sections
- Two-group discontinuity factors for the four radial sides and four radial edges of a node ( $f_g$ 's)
- Number of neutrons emitted per fission ( $\nu$ ), energy release per fission ( $\kappa$ ), and iodine and xenon fission yields ( $\gamma_i, \gamma_{Xe}$ )

Each of those variables is obtained by interpolation in cell data tables produced by PHOENIX. Cell data tables contain cross section values as functions of one or more parameters. Each of those parameters represents a physical quantity or phenomenon that influences the few-group cross sections:

- Burnup (E)
- Instantaneous Coolant Density ( $\rho$ )
- Coolant Density History ( $\rho_h$ )
- Control Rods (CR)
- Spacer Grids (SG)
- Control Blade History (CBH)
- Soluble Boron
- Fuel Temperature
- Xenon
- Heavy-metal and fission product nuclide inventory

The POLCA cross section model typically constructs a given quantity by mathematical representations such as the one illustrated here for macroscopic cross sections:

$$\begin{aligned} \Sigma = & \Sigma^{base}(E, \rho, \rho_h) + \Delta\Sigma^{CR} + \Delta\Sigma^{SG} + \Delta\Sigma^{Bor} \\ & + d_{Dop} \left[ \sqrt{T_f} - \sqrt{T_f^{ref}} \right] \\ & + \sum_i \sigma_i \left[ N_i - N_i^{ref}(E, \rho_h) \right] + \Delta\Sigma^{SpatialVar} \end{aligned} \quad \text{Eq. 4.1}$$

This cross section model is based on a combination of a “base” cross section and “difference” terms. The base cross sections,  $\Sigma^{base}$ , are computed by PHOENIX at “base conditions”. A base condition is defined as an exposure state (E) with a given instantaneous coolant density ( $\rho$ ) for a depletion case with a given coolant density history ( $\rho_h$ ), absence of control rods, no spacer grids, reference fuel temperature ( $T_f^{ref}$ ) and reference power density (yielding a reference Xenon equilibrium concentration  $N_{Xe}^{ref}$ ).

The difference terms represent perturbations of the base states with regard to the insertion of control rods ( $\Delta\Sigma^{CR}$ ) or spacer grids ( $\Delta\Sigma^{SG}$ ), or variations of boron concentration ( $\Delta\Sigma^{Bor}$ ) or fuel temperature ( $d_{Dop}[\sqrt{T_f} - \sqrt{T_f^{ref}}]$ ).

Depleting at conditions different from the reference conditions utilized in PHOENIX to generate the cell data results in an isotope inventory ( $N_i$ ) that differs from that which is obtained at reference conditions. POLCA accounts for this phenomenon by explicitly tracking all important nuclides ( $i$ ) and corrects for these isotopic deviations through the next-to-last term in Eq. 4.1.

Likewise, burnup induced intra-node effects are accounted for via a spatial variation correction term which is internally computed from isotopic and burnup information on the sides of all nodes ( $\Delta\Sigma^{\text{SpatialVar}}$ ). The spatial variation correction provides variations in spectral history relative to the history built into the base cross sections.

Cell data are normally represented by three dimensional tables with entries for  $E$ ,  $\rho_h$ , and  $\rho$ . **[PROPRIETARY INFORMATION DELETED]**.

For accurate evaluation of history effects, microscopic cross sections are needed. They are computed using the following equations:

$$\sigma_i = \sigma_i^{\text{base}}(E, \rho) + \Delta\sigma_i \quad \text{Eq. 4.2}$$

$$\Delta\sigma_i = \Delta\sigma_i^{\text{SG}} + \Delta\sigma_i^{\text{CR}} + \Delta\sigma_i^{\text{Bor}} + \Delta\sigma_i^{\text{Dop}} \quad \text{Eq. 4.3}$$

Microscopic cross sections are computed in much the same way as macroscopic cross sections, except that burnup induced effects as well as the nonlinear isotopic spectral effects are not considered to be required. **[PROPRIETARY INFORMATION DELETED]**.

#### 4.5 BWR THERMAL-HYDRAULICS MODEL

In a BWR core simulator program, the thermal-hydraulics model has a significant effect on the calculated core reactivity and power distribution. The neutronic and thermal-hydraulic models in POLCA are coupled through the power and void interaction encompassed in the power-void iteration loop of the code. This iteration uses the three-dimensional power distribution from the neutronics calculation directly in the evaluation of the three-dimensional void distribution. An iterative procedure is utilized until consistent power and void distributions are obtained from the calculations.

The thermal-hydraulic model is used to determine the distribution of pressure, enthalpy, temperature, coolant flow, coolant void, heat flux and critical power ratio (CPR) at steady-state conditions. Thermal-hydraulic initial conditions in the core are defined by such parameters as the thermal reactor power, total core recirculation flow, reactor pressure, and feedwater enthalpy, as well as the three-dimensional power distribution from the neutronics calculation. The total coolant flow entering the core is known in the POLCA hydraulics model. Computing the flow through each fuel assembly (channel) is a primary objective of the hydraulics calculation in POLCA.

The thermal-hydraulic model in POLCA is an updated version of the model contained in the original NRC accepted version of POLCA described in Reference 1. As discussed in Reference 1, this thermal-hydraulic model is the same as the CONDOR code described in Reference 20. The calculational approach and basic models described in Reference 20 have been retained. However, the hydraulic models have been improved to allow a more precise description of the individual fuel assemblies and the reactor core.

The general features of the hydraulic models described in References 1 and 20 are retained in POLCA. Specifically, the single-phase liquid, sub-cooled boiling, and bulk-boiling state flow regimes can be represented in the thermal-hydraulic model. Mass, energy, and momentum are conserved. Mass continuity is satisfied by requiring that the sum of all channel flows equal the total core flow. Energy conservation requires that energy delivered to the coolant in a given axial node divided by the flow rate in the node be equal to the enthalpy rise in the node. Momentum conservation is addressed by expressing the axial pressure drops in terms of elevation, acceleration, and friction pressure drops as well as local form losses. Bypass flows continue to be modeled in terms of pressure differentials as described in Reference 20. For a given three-dimensional core power, the calculation begins at the core inlet and continues, node by node, from the inlet to the outlet for each fuel assembly channel. The pressure drop across each node is evaluated, and when integrated over the length of the fuel assembly channel, yields the total pressure drop for the fuel assembly. Having obtained the total pressure drop for each fuel assembly, the core average pressure drop is computed, and the assembly flow distribution is evaluated. The code iterates on the flow distribution through each fuel assembly until the pressure drop calculated across each assembly is equal to the core average pressure drop. Having obtained a converged hydraulic solution for a given power distribution, the distributions of pressure,

enthalpy, temperature, coolant flow, and coolant void are established. The code iterates on the power and void distributions to obtain a converged solution.

As noted above, the hydraulic model in POLCA has been improved to allow a more accurate description of hydraulic characteristics of the reactor core and fuel assemblies. Specific improvements in the version of POLCA relative to that described in References 1 and 20 can be summarized as follows:

1. An option to describe additional leakage paths between the active coolant channel (the water directly surrounding the fuel rods in an assembly) and the inter-assembly bypass has been added.
2. The capability to more explicitly describe the axial variation of assembly designs has been added. For example, the flow area, hydraulic diameter and number and diameters of fuel pins in axial segments of the fuel assembly can vary. A more precise description of the fuel assembly geometry above the active fuel region has also been incorporated.
3. The water-steam properties needed in the thermal-hydraulic model are evaluated using the WADA subroutine package based on standard international steam table functions (Reference 21).
4. The size of the nodal mesh can vary axially.
5. Greater flexibility in modeling leakage flows between the active flow region and unheated flow channels within the assembly (e.g. water rods, SVEA water cross components, etc.) has been incorporated.
6. Inlet orifice and tie plate form loss coefficients have been generalized to optionally include a Reynolds number dependence.

The three-dimensional hydraulic model for the reactor core is based on a nodal mesh description similar to that used in the neutronics model. In the radial direction each node corresponds to a fuel assembly or an unheated flow channel consistent with the nodal geometry used in the neutronics model.

A variety of pressure drop correlations are available for use in POLCA to match performance data of specific fuel designs. [PROPRIETARY INFORMATION DELETED].

The combination of all pressure drop correlations used for a given assembly design is verified by comparison with performance data for that assembly design. As discussed in Reference 22, ABB test loop data are used to verify the use of the combination of pressure drop correlations in conjunction with form loss coefficients and flow hole sizes for ABB fuel designs. For non-ABB fuel co-resident in a mixed core containing ABB reload fuel, similar verification is performed based on **[PROPRIETARY INFORMATION DELETED]**.

Three-dimensional void distributions for subcooled and bulk boiling regimes continue to be calculated with drift-flux model correlations adjusted to fit experimental data. In addition to the Zuber-Findley type correlation adjusted to ABB test loop data discussed in Reference 20, available industry standard correlations are being added to the library of bulk void correlations as they become available. For example, the EPRI bulk boiling correlation has been added to the data base. In addition, additional FRIGG loop void measurements to augment the existing data base continue to be performed to improve the ABB capability to describe core void distributions. A given void correlation is qualified for a specific code application. In addition, a specific hydraulic model in POLCA in conjunction with the void correlation used is verified on a plant-specific basis for reload applications by performing core follow calculations to establish hot and cold reference values of  $k_{\text{effective}}$  and to verify that acceptable power shapes are predicted by comparison with TIP data.

#### 4.6 DETECTOR MODEL

The detector module of POLCA handles two types of response simulations for BWR in-core detectors:

- Neutron in-core detectors
- Gamma in-core detectors

The in-core neutron sensitive response calculation is based on computing the reaction rate induced in the detector by impinging neutrons. This is done by combining detector response functions ( $D_g^{\text{det}}$ ) generated by the lattice code with the point fluxes in the detector location ( $\phi_g^{\text{det}}$ ) computed by POLCA and summing over the energy groups ( $g$ ):

$$R_{\text{neutron}} = \sum_{g=1}^2 D_g^{\text{det}} \phi_g^{\text{det}} \quad \text{Eq. 4.4}$$

**[PROPRIETARY INFORMATION DELETED].**

The in-core gamma response is correlated to a weighted sum of the powers of the fuel pins in the bundles surrounding the detector with expressions of the form:

$$R_{\text{gamma}} = \sum_{K=1}^4 X_K \sum_{i=1}^N w_i^K p_i^K \quad \text{Eq. 4.5}$$

where  $X_K$  is the gamma detector constant for assembly  $K$ ,  $w_i^K$  is the importance weight for pin  $i$  with pin power  $p_i^K$  for assembly  $K$ . The pin powers, weighting factors, and detector constants are established by a combination of lattice code (e.g., PHOENIX) and POLCA calculations.

**[PROPRIETARY INFORMATION DELETED].** The total response at the gamma ray detector is computed by a weighted sum of contributions from different axial levels.

#### 4.7 ALBEDO MODEL

Two-group albedo boundary conditions are utilized on the outer surfaces of the reactor problem. The outer surfaces may be on the edge of the active core, [PROPRIETARY INFORMATION DELETED].

The boundary conditions of the three-dimensional core simulator are expressed by means of partial current albedos in two-energy groups:

$$j^{return} = \underline{\underline{a}} j^{out} \quad \text{Eq. 4.6}$$

where  $j$  represents two-group partial currents and  $\underline{\underline{a}}$  is the albedo matrix,

$$[\text{PROPRIETARY INFORMATION DELETED}] \quad \text{Eq. 4.7}$$

[PROPRIETARY INFORMATION DELETED]. The albedo concept may be utilized to express a number of special boundary conditions:

- Perfectly reflective boundaries are obtained by setting  $\underline{\underline{a}} = \underline{\underline{I}}$
- Zero net current boundary conditions are described by  $\underline{\underline{a}} = 0$ .
- Zero flux boundary conditions are obtained if  $\underline{\underline{a}} = -\underline{\underline{I}}$

The reflector region may be described purely by albedos or, [PROPRIETARY INFORMATION DELETED].

#### 4.8 XENON TRANSIENT MODEL

For reactor transients on the time scale of hours, Iodine and Xenon are calculated in separate depletion chains. Two calculational capabilities exist in POLCA. These are the equilibrium Xenon feedback and the Xenon short term time stepping options. The latter can be used to obtain non-equilibrium I-135 and Xe-135 distributions, following a short time step and assuming other nuclide concentrations remain constant. Xenon time stepping combined with successive flux calculations is used to calculate Xenon transients over periods of several hours following a change in operating conditions such as power level or rod bank insertion.

[PROPRIETARY INFORMATION DELETED].

#### 4.9 PIN POWER RECONSTRUCTION MODEL

Design and licensing analyses require local rod power distributions to establish the following types of quantities:

- Local peaking factors
- Thermal quantities such as Linear Heat Generation Rate (*LHGR*), Average Planar Linear Heat Generation Rate (*APLHGR*) and surface heat flux (*SHF*)
- Critical power ratio input parameters to account for individual rod powers such as R-factors
- Detector response
- The tracking of individual pin powers, pin burnup, and fast neutron fluence for various applications such as establishing *PCI* conditioning and deconditioning profiles and supporting fuel rod performance calculations

Since POLCA is a coarse mesh method, its primary function is the calculation of nodal powers resulting in dependent variables which are averaged over individual nodes. Calculation of local pin powers with traditional core simulators, such as the POLCA version described in Reference 1, has involved combination of the nodal powers calculated with the core simulator with the unperturbed pin powers established with the lattice code. This option continues to be available with the version of POLCA described in this report. In addition, the POLCA version described herein allows correction of local pin powers calculated with the lattice code based on the results of the nodal calculation performed with POLCA. This correction is referred to as pin power reconstruction.

The pin power reconstruction process involves the superposition of heterogeneous information from the lattice code with a smoothly varying homogeneous power distribution determined from POLCA to obtain a composite power distribution on the pellet level. Specifically, the local (i.e., pellet level) power distribution is given by:

$$P(x, y, z) = S_{rad}(x, y) S_{ax}(z) P^{hom}(x, y, z) \quad \text{Eq. 4.8}$$

In Equation 4.8,  $S_{rad}(x,y)$  is the radial fine structure shape function (one value per fuel rod at a given axial height) carried over from the lattice code calculation. This function accounts for the heterogeneous nature of relative rod power distribution due to such effects as individual pin enrichments and the local effects of control rods. The effect on the radial shape function of control blade history (CBH) is discussed in Section 4.9.2.

The term  $S_{ax}(z)$  is the axial fine structure shape function. This factor accounts for axial heterogeneities such as spacers, control rod tips and enrichment and burnable absorber axial variations. The calculation of  $S_{ax}(z)$  is performed in POLCA as discussed in Section 4.10.

The last term,  $phom(x,y,z)$ , is the “homogeneous” power distribution inside a node obtained by solving the two-group diffusion equation with realistic boundary conditions [PROPRIETARY INFORMATION DELETED]. It accounts for global, smooth power variations from such effects as the uneven leakage of neutrons from neighboring nodes operating at different powers and by the fact that the assemblies are depleted in a different environment in the reactor than assumed in the lattice code simulation.

Equation 4.8 makes the basic assumption that the radial and axial heterogeneous dependencies are separable.

#### 4.9.1 Radial Shape Function

The radial shape function in Equation 4.8 is not necessarily equal to the pin power solution  $P_{LC}^{het}(x,y)$  of the lattice code but is given in general by:

[PROPRIETARY INFORMATION DELETED]. Eq. 4.9

[PROPRIETARY INFORMATION DELETED].

#### 4.9.2 Control Rod History and the Radial Shape Function

Operation of BWRs with control rods inserted in the core gives rise to a strong buildup of plutonium in the vicinity of the control rod blades as well as a retarded depletion of fuel pins. As a consequence, the power in the pins adjacent to the control rod may increase substantially when the control rod is withdrawn after extended periods of operation with the control rod inserted. Subsequent depletion without the presence of control rods causes these peak pins to deplete faster than the average pin causing the effect of

the control rod insertion to diminish as the assembly is depleted. This phenomenon is widely known as the control blade history (CBH) effect. In POLCA, the CBH effect is addressed in terms of the buildup phase when the control rod is inserted and the decay phase after the control rod is removed.

The effects of control rods on local pin power distributions are treated in POLCA as **[PROPRIETARY INFORMATION DELETED]**.

#### 4.10 AXIAL HOMOGENIZATION

Material variations within the axial nodes can lead to important reaction rate and flux variations which would not be captured by traditional node average fluxes. Spacers, control rod tips, burnable absorber variation, enrichment zoning, and reflector regions at the assembly ends are examples of those material variations.

The nodal cross sections used by POLCA account for the presence of axial heterogeneities through axial homogenization corrections derived from an axial homogenization method included in POLCA. This method also yields axial discontinuity factors which provide neutron balance in the presence of axial material variations within the node and are utilized in the nodal coupling coefficients. The POLCA treatment of the axial variations also provides a smoothly varying axial flux which can be used to correct the axial power distributions with the axial fine structure function discussed in Section 4.9 to accommodate the heterogeneous variations within the node (i.e.,  $S_{ax}(z)$  in Equation 4.8).

While inhomogeneous radial effects within the nodes require heterogeneous input from the lattice code, inhomogeneous axial variations are treated entirely within POLCA with a sophisticated axial homogenization procedure. **[PROPRIETARY INFORMATION DELETED]**.

## 4.11 DEPLETION CALCULATIONS

POLCA has the capability to track concentrations of important isotopes, as well as burnups from core average to the local level, core resident times (effective full power hours), moderator density history, and control blade history in support of design and licensing analysis applications.

The nuclide concentration capability is described in Section 4.11.1. Various burnups (e.g. nodal, rod average, and assembly average) are used, for example, as independent variables for specifying thermal limits. Moderator density history is an independent variable for the determination of macroscopic cross sections. Control blade histories are used to establish the effects of depletion due to control blades.

In addition, while not typically required for reload design and licensing applications, control rod depletion and fuel channel fluence information is tracked. The following control rod information is compiled to support evaluation of the effects of neutron irradiation on their reactivity worth and structural integrity, and hence aid in control rod management decisions:

- effective full power hours of core residence
- depletion fraction of the active control rod material
- fast neutron fluence of the control rod structural material (including the handle)

Channel fluence and residence time can be useful for understanding channel behavior and channel management. Therefore, the fast fluence distribution and core residence time for each fuel channel are tracked.

As discussed in Section 4.11.2, detector depletion is also followed in POLCA.

### 4.11.1 Nuclide Concentration Tracking

The important time dependent nuclide concentrations dealt with in POLCA can be divided into two groups. The first group contains the Iodine and Xenon depletion chains and involves time constants in terms of hours. Calculation of time dependent Iodine and Xenon concentrations is addressed in Section 4.8. The second group involves isotopes whose buildup and decay is described with time constants at least as large as days. This section deals with isotopes which are in the second group.

The most important heavy nuclides and fission products are tracked explicitly in POLCA. The processes in the mathematical model for the transmutation of nuclides include both production and destruction mechanisms.

For example, nuclide  $i$  can be assumed to be produced through a combination of three mechanisms

- direct fission (fission yield  $\gamma_i$ )
- $\beta$ -decay of its predecessor  $i-1$  (decay constant  $\lambda_{i-1}$ )
- conversion (microscopic capture cross section  $\sigma_{c,i-1}$ )

Nuclide  $i$  can be assumed to be removed from the system through

- $\beta$ -decay
- neutron absorption

Assuming a two neutron energy group model, the depletion process can be described by the number density equation:

$$\begin{aligned} \frac{dB_i}{dt} = & \gamma_i (\Sigma_{f1}\phi_1 + \Sigma_{f2}\phi_2) + \lambda_{i-1}A_{i-1} \\ & + (\sigma_{c1,i-1}\phi_1 + \sigma_{c2,i-1}\phi_2)B_{i-1} \\ & - \lambda_i B_i - (\sigma_{a1,i}\phi_1 + \sigma_{a2,i}\phi_2)B_i \end{aligned} \quad \text{Eq. 4.10}$$

**[PROPRIETARY INFORMATION DELETED].**

The isotopes currently selected for explicit representation in POLCA are shown in Appendices B and C. These isotopes are a subset of the set of isotopes provided in the PHOENIX library. The isotopes which are not explicitly treated in POLCA are accounted for in macroscopic cross sections input to POLCA. The macroscopic cross sections input to POLCA are described in Section 4.4.

Examples of the criteria used for selecting nuclides for explicit representation in POLCA are:

| - [PROPRIETARY INFORMATION DELETED]

#### 4.11.2 Detector Depletion

POLCA tracks the depletion of fission chamber type neutron detectors. The active fissionable material in these detectors consists of U-235. Such detectors may be enriched in U-234 to prolong the effective lifetime of the detector through U-235 breeding. The depletion state of a detector accordingly can be represented by the following:

| - [PROPRIETARY INFORMATION DELETED]

#### 4.12 POWER PEAKING FACTORS AND THERMAL MARGINS

POLCA edits power peaking factors and distributions as well as parameters used to monitor margins to thermal limits. These parameters can be divided into four categories:

1. Assembly, nodal, and local power peaking factors and power distributions are edited by POLCA to assist in the design process and to support a thorough understanding of the core behavior. These quantities are calculated in POLCA from the power distributions calculated by POLCA as well as those predicted by the lattice code. Power distributions calculated in POLCA are also used in the evaluation of thermal margins and performance relative to PCI guidelines.
2. Fission heat load quantities used for monitoring margins to licensing analysis limits are calculated by POLCA. These parameters include quantities such as Linear Heat Generation Rate (LHGR) and Average Planar Linear Heat Generation Rate (APLHGR).
3. Critical power ratio (CPR) is calculated by POLCA. Examples of the use of this parameter includes comparison with CPR limits during the design process and establishment of CPR limits for anticipated operational occurrences and accidents which can be treated with steady-state methods using the methods described in Reference 22.

4. Parameters which are used to implement guidelines recommended to protect against Pellet-Clad Interaction (PCI) are input to POLCA. These parameters include specification of PCI thresholds as well as ramp rate and conditioning restrictions. Utilizing these parameters, POLCA calculates conditioning and deconditioning profiles which can be used in the design phase to predict the impact of the PCI guidelines on core operation.

#### 4.12.1 Power Peaking Factors and Distributions

The POLCA calculational methods described in Sections 4.1 through 4.11 provide power distributions from assembly to pin level. These power distributions can be studied directly in the design phase, used to establish a variety of peaking factors which reflect the behavior of the core, or used to establish parameters such as LHGR, APLHGR, and CPR upon which BWR thermal limits are typically based. A broad editing capability allows consideration of all power distributions required by the analyst from the assembly level to the pin level.

In addition, a broad range of quantities which indicate the characteristics of power distributions are available. The following are examples of these parameters:

- Relative nodal power density
- Core power axial offset
- Relative pellet peaking factor within a node
- Relative pin peaking factor within an assembly
- Maximum pin peaking factor within a node
- Assembly R-factors used in CPR correlations
- Maximum relative power density of any node in the core
- Maximum relative power density of any assembly in the core
- Maximum relative power in average axial power profile

#### 4.12.2 Fission Heat Load Calculations

Fission heat load parameters are typically used to establish thermal margins and are derived directly from power distributions.

The Linear Heat Generation Rate (LHGR) for a node is defined as the maximum pellet power transferred from the fuel to the coolant per unit length. LHGR is a measure of the fission heat load of a fuel pin. LHGR is one of the parameters typically used to assure that fuel rod thermal-mechanical design criteria are satisfied.

The LHGR is calculated in POLCA as follows:

$$LHGR = Q_{rel} * P * F_{xyz} * \pi_v h_x^2 * (1-\gamma) / N_f \quad \text{Eq. 4.11}$$

where

$Q_{rel}$  = Relative core thermal power

$P$  = Node power density relative to the entire core

$F_{xyz}$  = Pellet power peaking factor relative to all the pellets in the node. [PROPRIETARY INFORMATION DELETED]

$\pi_v$  = Nominal volumetric core power density (W/m<sup>3</sup>)

$h_x$  = Nodal width

$\gamma$  = Fraction of fission power deposited outside the fuel pin via gamma and neutron radiation

$N_f$  = Number of fuel pins in node

Ratios of LHGR to the LHGR limit typically based on thermal-mechanical design criteria are calculated and edited to allow monitoring of margin to the thermal limit.

The Average Planar Linear Heat Generation Rate (APLHGR) for a node is defined as the heat conducted from the fuel to the coolant averaged over the fuel rods in the node at the elevation in the node at which the APLHGR is a maximum:

$$APLHGR = Q_{rel} * P * F_z * \pi_v h_x^2 * (1-\gamma) / N_f \quad \text{Eq. 4.12}$$

where the quantities common to Equation 4.11 and 4.12 have the same meaning, and

$F_z$  = Power axial peaking factor in the node relative to the nodal power

Ratios of APLHGR to the APLHGR limit which typically assures that acceptance criteria for postulated Loss of Coolant Accidents are satisfied are edited to allow monitoring of margin to the thermal limit.

#### 4.12.3 Critical Power Ratio

BWR fuel assemblies are operated in a manner which assures that boiling transition can occur in fewer than 0.1% of the fuel rods for normal operation and postulated anticipated operational occurrences. Thermal margin to boiling transition is evaluated in BWRs with the Critical Power Ratio (CPR). The CPR is defined as the ratio of the assembly power required to initiate boiling transition anywhere in the assembly to the power at which the assembly is operating. CPR correlations appropriate for each unique assembly type in the core are included in POLCA. Examples of CPR correlations for ABB fuel are found in References 23 and 24. The CPR associated with each core location is compared with the CPR limit for the assembly type in that location, and margins to the limit are edited.

#### 4.12.4 Pellet-Clad Interaction

Pellet-clad interaction (PCI) surveillance is performed by monitoring the conditioning and deconditioning of the fuel to allow a given LHGR. A check is performed to determine whether the actual LHGR exceeds the level to which the fuel has been conditioned. PCI tracking is done for any number of user specified fuel pins in each assembly.

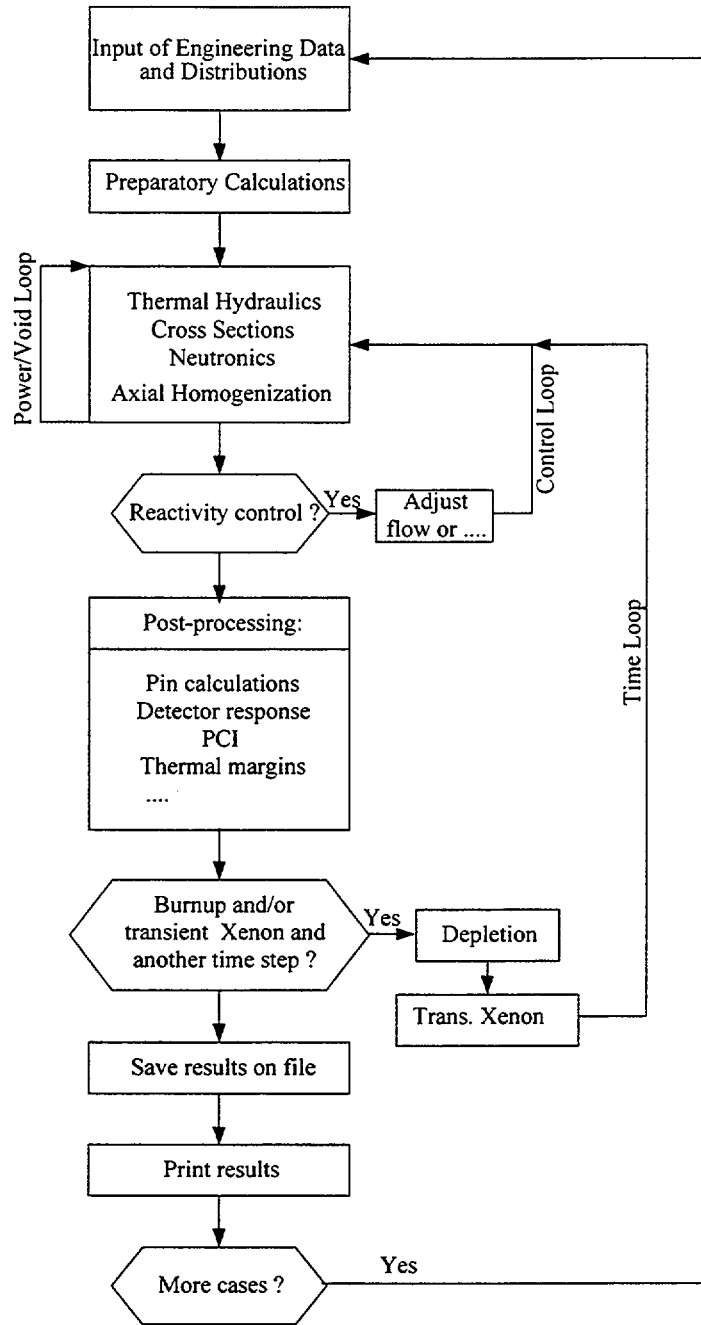


Figure 4.1: POLCA Calculation Flow Diagram

## 5.0 POLCA QUALIFICATION

The qualification of POLCA is divided into two categories referred to as verification and validation. In the context of this report, verification involves the testing of individual models or combinations of models to verify that they perform as intended. Validation involves the comparison of POLCA predictions with measured data to establish the accuracy of the system operating as a whole.

The POLCA verification is performed by comparison with computational benchmarks generated by means of reference calculations as well as by comparison with experimental data suitable for evaluating the individual model being verified. Specifically, the POLCA verification effort covers the three areas listed below:

- The neutronics model is verified by comparison with established two-dimensional analytical benchmarks. Three of the analytical benchmarks involve power calculations without depletion for both PWR and BWR cores. The fourth benchmark provides verification of the POLCA depletion models.
- Verification of the thermal-hydraulic model in Reference 20 is augmented by comparisons with test loop pressure drop measurements and individual channel flow measurements in a Nordic BWR.
- The POLCA pin power reconstruction model is verified by comparison with a pin power distribution benchmark. Furthermore, the capability of POLCA to predict relative nodal fuel pin and fuel rod power distributions is verified by comparisons with fuel rod gamma scan data.

The POLCA validation involves the evaluation of core follow predictions for four reactors as well as comparisons with gamma scan measurements. Specifically,  $k_{\text{effective}}$  values calculated by POLCA are evaluated, and measured in-core detector responses and measured gamma scan data are compared with POLCA predictions. The gamma scan, reactivity and TIP data were obtained from four BWRs:

- Plant A (ABB built internal pump plant): Predicted  $k_{\text{effective}}$  values are evaluated, and measured Traversing In-core Probe (TIP) data are compared with POLCA predictions. Bundle and individual fuel rod gamma scan measurements are compared with POLCA predictions.

- Plant B (GE built BWR/6): Predicted  $k_{\text{effective}}$  values are evaluated, and measured TIP data are compared with POLCA predictions. Bundle and individual fuel rod gamma scan measurements are compared with POLCA predictions.
- Plant C (ABB built internal pump plant): Predicted  $k_{\text{effective}}$  values are evaluated, and measured TIP data are compared with POLCA predictions.
- Plant D (GE built BWR/4): Predicted  $k_{\text{effective}}$  values are evaluated, and measured TIP data are compared with POLCA predictions.

## 5.1 NEUTRONIC MODEL VERIFICATION

Comparisons of the POLCA neutronic model calculations with reference solution results for four benchmark problems are discussed in this section. The analytical nodal method in POLCA is extensively tested by each of these benchmarks.

### 5.1.1 IAEA Benchmark

The International Atomic Energy Agency (IAEA) two-dimensional benchmark problem specified in Reference 25 was evaluated with POLCA. The identifier in Reference 25 for this problem is 11-A2. This benchmark consists of two different fuel bundle types with reflector bundles on the edges of the core and a total of 177 assemblies. The configuration is one-eighth core symmetric. Each assembly has a width of 20 cm and a height of 340 cm. The fuel and reflector bundles have no internal pin structure, and are represented by uniform two-group cross sections. The large flux gradients in the vicinity of the reflector and near the control rods provide a very good test for a code such as POLCA.

The relative assembly powers and  $k_{\text{effective}}$  predicted by POLCA were compared with a benchmark reference solution for this configuration. In the discussion below, the term "error" refers to the magnitude of the difference between the relative assembly power predicted by POLCA ( $P$ ) and the relative assembly power predicted by the reference solution ( $P_{\text{ref}}$ ).

The POLCA solution for this benchmark was compared with Solution 3 (i.e., 11-A2-3) in Reference 25. This solution utilized a nodal method referred to as the nodal expansion method which was run on a very refined spatial mesh (36 meshes per assembly) and should provide a very accurate solution to this problem.

The results obtained with POLCA are compared with those predicted by solution 11-A2-3 in Figure 5.1. Relative to solution 11-A2-3, the POLCA solution has **[PROPRIETARY INFORMATION DELETED]**.

The conclusion from the two-dimensional IAEA benchmark is that the two computations (POLCA and Solution 11-A2-3 in Reference 25) yield virtually identical results. The small differences observed are characteristic of expected numerical deviations. Overall, this benchmark comparison is a strong indication that the analytical nodal method has been correctly implemented in POLCA and is performing as intended.

### 5.1.2 BIBLIS Benchmark

As discussed in Reference 26, the BIBLIS benchmark is a two-dimensional model of an operating PWR core with a multi-zone, checkerboard loading. This configuration is one-eighth core symmetric with seven different homogenized fuel compositions and a homogenized reflector. Each assembly has a width of 23.1 cm. The realistic nature of this problem makes it a good test for the POLCA neutronics model which will provide errors or uncertainties similar to those expected in practice. The fact that it is not a BWR core does not diminish its value as a verification of the correct implementation of the analytical nodal method since all fuel bundles have been homogenized.

The POLCA solution was compared with a reference solution generated with the code LABAN as reported in Reference 26. The results obtained with POLCA are compared with those predicted by LABAN in Figure 5.2. Relative to this benchmark, the POLCA solution has **[PROPRIETARY INFORMATION DELETED]**.

The agreement between the results from POLCA and LABAN are considered to be very good recognizing the realistic nature of the configuration. Therefore, this benchmark comparison corroborates the correct implementation of the analytical nodal method in POLCA and demonstrates that the model is performing as intended.

### 5.1.3 DVP Benchmark

The DVP problem described in Reference 27 is a two-dimensional BWR case that includes assembly discontinuity factors (ADFs). It is included in this section to demonstrate the ability of POLCA to use ADFs. The core contains three different fuel bundle types with reflector assemblies described as a fourth material. Each assembly has a width of 15.3 cm. The problem is analyzed with zero flux boundary conditions on the outer edge of the reflector. This benchmark was originally defined with multiple reflector layers. For the POLCA evaluation, the problem was modeled with only one reflector layer.

Since the objective of this calculation is to test the implementation and use of ADFs in POLCA, the results calculated with POLCA were compared with the results calculated with an independent advanced nodal method code which also uses ADFs. Accordingly, the MGRAC code described in Reference 28 was used to provide the reference results for comparison with the POLCA results.

The maximum difference in relative assembly powers predicted by POLCA and MGRAC was [PROPRIETARY INFORMATION DELETED]. The standard deviation in the relative difference in assembly relative powers was [PROPRIETARY INFORMATION DELETED]. The two codes predict a difference in  $k_{\text{effective}}$  of [PROPRIETARY INFORMATION DELETED]. The very small differences confirm that the implementation and use of ADFs is the same in both codes. Therefore, they confirm the correct application of ADFs in POLCA.

Reference 27 also provides a fine mesh reference solution in the form of a two-group, PDQ calculation which explicitly modeled all fuel pins, water gaps, control blades and the reflector. PDQ is a diffusion theory code with a very fine mesh capability which provides a finite difference solution to the diffusion equation. Comparison of the POLCA results for this benchmark with the PDQ results provides an additional test of the overall performance of the POLCA analytical nodal method with ADFs.

Figure 5.3 shows the differences between the relative assembly powers predicted by POLCA and PDQ. The differences shown in Figure 5.3 are similar to those between PDQ and other state-of-the-art analytical nodal method applications as discussed in Reference 27. Therefore, the comparison in Figure 5.3 further confirms that the analytical nodal method model has been properly implemented in POLCA and is performing as intended.

#### 5.1.4 Intra-Nodal Depletion Benchmark

This benchmark is a two-dimensional, two-group, two cycle depletion test case with octant symmetry. It differs from the other computational benchmarks in that it is a test of the coarse mesh modeling of core depletion as well as the computation of the intra-nodal spatial burnup distribution. This benchmark is described in Reference 29 and the identifier given to this problem there is Case 19. Although the core geometry is typical of PWRs, this benchmark is also relevant for BWRs since it tests the ability of the neutronic model to accurately calculate the intra-nodal burnup distribution and to account for its effects on the core wide power distribution and reactivity.

One third of the core is reloaded at the beginning of the second cycle. Control rods are fully withdrawn during depletion, and the reactor is maintained critical with soluble boron. The length of each cycle is determined by requiring the critical boron at end-of-cycle (EOC) to be zero.

The reference solution to which POLCA is compared in this case is Solution 19-A1-1 in Reference 29. As discussed in Reference 29, this reference solution was obtained by solving the two-group diffusion equation with the nodal expansion method (NEM) with fourth order polynomials and a quadratic transverse leakage approximation. Each assembly was modeled as a 5x5 nodal array in the radial direction in the reference solution. Therefore, this reference solution is judged to provide a sufficiently rigorous flux solution and sufficient intra-nodal detail to provide a good benchmark for POLCA.

In order to capture sufficient intra-assembly detail for meaningful comparison with the reference case, each assembly was described as a 2x2 nodal array radially in POLCA. This option is available in POLCA for PWR applications. Due to the relatively small assembly dimensions in BWRs, this capability is not considered to be required for BWR applications. The assembly pitch in U.S. BWRs is 15.2 cm. Since the 2x2 subdivision in this PWR case results in a 11.5 cm radial mesh, the suitability of this case as a POLCA benchmark for BWR applications is improved by the 2x2 subdivision in the POLCA model.

Tables 5.1 and 5.2 provide statistics reflecting the relative differences in nodal powers predicted by POLCA and those predicted by the reference case as well as the difference in the prediction of critical boron concentration for the control rods inserted and withdrawn. Rod worth (RW) comparisons are provided in Table 5.3.

The quarter core relative power distribution predicted by the reference solution and the difference in relative power between the POLCA prediction and the reference solution corresponding to the case presented in Table 5.1 (Cycle 1, rods out) are shown in Figure 5.4.

As shown in Tables 5.1 and 5.2 and Figure 5.4, the relative powers and reactivity levels predicted by POLCA are in good agreement with those predicted by the reference solution. The slightly better agreement in the case with control rods withdrawn is consistent with the steeper flux gradients caused by the insertion of control rods. Table 5.3 shows that control rod worths predicted by POLCA are also in good agreement with those predicted by the reference solution. Therefore, the comparisons between the POLCA and reference solution for this benchmark provide confirmation that the advanced nodal method and the POLCA depletion models have been correctly installed in POLCA and are performing as intended.

## 5.2 THERMAL-HYDRAULICS MODEL VERIFICATION

As discussed in Section 4.5, the thermal-hydraulic model in POLCA is an updated version of the model contained in the original version of POLCA described in Reference 1. This thermal-hydraulic model is a version of the CONDOR code described in Reference 20 which was made an integral part of the POLCA version described in Reference 1. Therefore, the qualification measures discussed in Reference 20 also provide verification of the new POLCA version discussed in this report. For example, pressure drop predictions with CONDOR are compared with an exact analytic solution for a simple case in Reference 20. Specifically, analytic integration of the pressure drop equation in the code for the simple case of homogeneous two-phase flow in a vertical heated tube assuming the steam and liquid phases have the same velocity were compared with the code predictions. The excellent agreement between the code predictions and the analytic solution applies to the hydraulic model in the POLCA version described in this report since the hydraulic model in POLCA is identical to the model described in Reference 20 for the simulation of the analytic solution.

Benchmarking of the hydraulic model in POLCA has been expanded by comparing POLCA predictions with additional, more recent test loop data and in-core measurements. Specifically, this section contains comparisons of POLCA predictions with FRIGG Loop two-phase pressure drop measurements and assembly flows measured in an ABB Nordic reactor.

The POLCA calculations referred to in Sections 5.2.1 and 5.2.2 were performed with the same void correlation discussed in Section 4 of Reference 20. Since the thermal-hydraulic models in POLCA are fundamentally the same as those in the POLCA version documented in Reference 1, the same level of accuracy in predicted void distributions quoted in Section 4 of Reference 20 can be expected in the calculations in Sections 5.2.1 and 5.2.2. While this level of accuracy is considered to be adequate, ABB maintains a continuing program to improve analytical methods. Accordingly, void measurements using test sections representative of current and advanced 10x10 SVEA designs are currently being performed. It is anticipated that these data will be used to further optimize void predictions for the 10x10 SVEA geometry.

### 5.2.1 Pressure Drop Comparisons

Axial pressure drop measurements are routinely performed for ABB assembly designs to establish local form loss coefficients and qualify two-phase multiplier and void correlations for specific assembly designs and code systems. These data are frequently obtained in conjunction with Critical Power tests. The pressure drops predicted by POLCA were compared with pressure drop measurements obtained for a 24-rod SVEA-96S subbundle in the ABB FRIGG Loop. With the exception of the fuel rod pitch, the SVEA-96S subbundle is the same as the SVEA-96+ subbundle described in Reference 24. A SVEA-96 type assembly contains four 24-rod subbundles which are mechanically identical. The SVEA-96S assembly is designed for ABB BWRs and has **[PROPRIETARY INFORMATION DELETED]** the SVEA-96+ assembly designed for use in U.S. BWRs.

Figure 5.5 is an axial sketch of the test assembly used for the pressure drop measurements showing the locations of the spacers and the pressure taps. The data were obtained for system pressures **[PROPRIETARY INFORMATION DELETED]** and a range of inlet subcooling temperatures **[PROPRIETARY INFORMATION DELETED]**. The range of test section flows **[PROPRIETARY INFORMATION DELETED]**.

Figure 5.6 provides comparisons between measured pressure drops and those predicted by POLCA over the range of system pressure, inlet subcooling, and test section flow rate. The pressure drops shown in Figure 5.6 are from the DP-12 cell at an elevation **[PROPRIETARY INFORMATION DELETED]** above the Beginning-of-Heated Length (BHL) to the DP-22 cell **[PROPRIETARY INFORMATION DELETED]**.

**DELETED]** shown in Figure 5.5. The relative error in the predictions relative to the measurements has a mean value **[PROPRIETARY INFORMATION DELETED]**. The relative error,  $\varepsilon$ , is given by

$$\varepsilon = \frac{P - M}{M} \times 100 \quad \text{Eq. 5.1}$$

where P is the value predicted by POLCA and M is the measured value.

This agreement between the POLCA predictions and the experimental data is considered to be very good. Therefore, the agreement between the measurements and POLCA predictions in Figure 5.6 provide general confirmation that the thermal-hydraulic models in POLCA are capable of accurately predicting local and overall pressure drops in a typical BWR assembly. Figure 5.6 also provides specific confirmation that the thermal-hydraulic models in POLCA, in conjunction with the void correlation and two-phase multiplier correlation utilized for this assembly design, accurately predict local and overall pressure drops for this design in POLCA.

### 5.2.2 Assembly Flow Rate Comparisons

The core flow rates in the newer ABB built BWR reactors in the Nordic countries are established from flow measurements at the entrance to eight individual assemblies. The existence of these instrumented assemblies also provides the opportunity of comparing calculated and measured assembly flow rates for an operating reactor. Accordingly, measured assembly flow rates for the eight instrumented locations in one of these modern ABB built BWRs were compared with POLCA predictions for those locations as a function of cycle burnup for several cycles. A POLCA simulation of each state point initiated from the POLCA core follow depletion was performed. The comparisons were made at state points for which TIP measurements were performed to assure that the core was at, or very close to, equilibrium conditions. At each point, the error,  $\varepsilon$ , in the predicted assembly flow rate relative to the measured assembly flow rate was established for each of the eight locations. The error has the same definition given in Equation 5.1 with P and M referring to assembly flow rates rather than pressure drops. In this case, the eight values of P and M at each point are normalized to the measured average over the eight locations.

The relative Root Mean Square Error (RMSE) at each state point is plotted in Figure 5.7. RMSE is defined here by:

$$RMSE = \sqrt{\frac{\sum_{i=1}^8 \varepsilon_i^2}{8}} \quad \text{Eq. 5.2}$$

As shown in Figure 5.7, the RMSE is [PROPRIETARY INFORMATION DELETED]. The RMSE over all the data is [PROPRIETARY INFORMATION DELETED]. It should be noted that the span of assembly flows (12.7 to 17.9 kg/s) in the eight locations over the 7 cycles shown in Figure 5.7 is substantial due to the large range of relative assembly powers. Therefore, the range of flow rates in the eight locations over this data base is considered to be representative of flow rates in potentially limiting assemblies at rated conditions in typical BWRs. The relatively small RMSE demonstrates that POLCA is predicting relative assembly flows with a high degree of accuracy. Therefore, these results also provide further confirmation that the hydraulic model in POLCA is providing an accurate simulation of the hydraulic performance of a BWR core.

### 5.3 PIN POWER CALCULATIONAL CAPABILITY QUALIFICATION

The capability of the pin power reconstruction model in POLCA to accurately predict pin powers is demonstrated in this section by comparisons of POLCA predictions with the results of a higher order reference solution for a hypothetical 17x17 PWR core. In addition, the overall capability of POLCA to predict fuel pin powers in operating BWR cores is confirmed by comparisons of POLCA predictions with fuel rod gamma scan measurements performed at two European reactors.

#### 5.3.1 NEACRP-L336 Benchmark

This section contains POLCA predictions of pin powers for the C3 configuration in the collection of NEACRP-L336 benchmarks described in Reference 30.

The C3 NEACRP-L336 benchmark is an infinite checkerboard core consisting of 2x2 arrays of unrodded UO<sub>2</sub> and MOX 17x17 assemblies. This configuration is shown in Figure 5.8. This benchmark can be used to test the pin power reconstruction capabilities of modern nodal codes.

The reference results to which the POLCA predictions were compared were calculated with the MGRAC code discussed in Reference 28. The MGRAC code is a multi-dimensional diffusion code with fine mesh capability. MGRAC also has the capability to generate the equivalent node-average quantities required by POLCA. Utilization of these equivalent nodal quantities in POLCA and subsequent comparison with the MGRAC fine mesh solution isolates the pin power capability of POLCA and allows a specific test of that capability without contamination by depletion and thermal-hydraulic feedback effects.

The reference results were generated by means of heterogeneous calculations in which each pin cell was explicitly modeled using an analytic nodal model and a mesh structure corresponding to 4 mesh points per pin cell. Auxiliary calculations with 25 mesh points per pin cell yielded differences of about 1 pcm in  $k_{\text{effective}}$  and 0.1% in pin powers indicating that the mesh structure used is sufficient to yield an accurate, spatially converged diffusion theory reference solution.

The POLCA model described each assembly as four nodes in a 2x2 array. Sensitivity calculations with a single node per assembly demonstrated that the two nodalization schemes did not yield markedly different results for realistic conditions.

Figures 5.9 and 5.10 provide detailed comparisons of the reference solution and POLCA results for the UO<sub>2</sub> and MOX assemblies, respectively. Each square in Figures 5.9 and 5.10 represents a location in the 17x17 array. The shaded non-central locations are control finger guide tubes, while the central shaded location is an instrument guide tube. The reference pin power, the predicted POLCA pin power, and the difference in the powers predicted by POLCA and the reference solution are listed in each of the fuel rod locations. Table 5.4 summarizes the results. Pin powers are normalized to an average of 1.0 for all fuel rods in the assembly array shown in Figure 5.8.

The comparisons in Figures 5.9 and 5.10 and Table 5.4 indicate that the POLCA pin power reconstruction models are providing accurate results and are performing as expected.

### 5.3.2 Fuel Rod Gamma Scans

This section contains comparisons of relative pin powers predicted by POLCA with gamma scan measurements of fuel rods in operating reactors. Comparisons are performed for fuel rods in three assemblies that were depleted at relatively high powers in a manner which might be expected for potentially limiting assemblies.

Fuel rod gamma scan measurements were performed at a Nordic BWR during the annual shutdown after 8 cycles of operation. This Nordic plant is a 500 assembly, 2500 MW<sub>th</sub> internal pump BWR designed by ABB. The gamma scan measurements were performed on 30 fuel rods of a SVEA-64 assembly after a single cycle of operation. The SVEA-64 assembly is a 64 rod assembly equipped with a water cross. The water cross in the SVEA-64 design delivers non-boiling water to the internal part of the assembly in a manner similar to the SVEA-96 design described in Appendix D2 of Reference 22. The SVEA-64 design contains four 4x4, 16-rod subbundles rather than the four 24-rod subbundles in the SVEA-96 assembly. The assemblies were identified as ADA005 and ACA001.

Fuel rod gamma scan measurements were also performed at a European BWR during the annual shutdown prior to Cycle 11. This plant is a 648-assembly, 3138 MW<sub>th</sub> GE designed BWR/6. Comparisons with POLCA predictions are shown for a total of 50 individual fuel rods from two SVEA-96 fuel assemblies with burnups of **[PROPRIETARY INFORMATION DELETED]**.

During the measurements, each fuel rod is gamma scanned in a special fixture over the entire length of the fuel rod. The intensities of the 1596-keV gamma rays from the decay of La-140 are measured. The La-140 activity can be used to establish the concentration of Ba-140. Since Ba-140 is a direct fission product with a well known yield, the Ba-140 concentration provides a reliable indication of relative power prior to shutdown. Consequently, the relative intensity of the 1596-keV gamma rays measured for the fuel rods can be assumed to reflect relative pin powers.

Since the POLCA predictions are based on core-follow calculations at actual plant conditions, comparisons of the POLCA results with the gamma scan measurements provide a reliable means of evaluating the capability of the PHOENIX/POLCA code system to predict local power within the limits imposed by the experimental uncertainties. The comparisons in this section are provided in terms of the parameter,  $\epsilon$ , where  $\epsilon$  is defined by:

$$\epsilon_{nk} = p_{nk}^c - p_{nk}^m \quad \text{Eq. 5.3}$$

where  $p_{nk}^c$  and  $p_{nk}^m$  are the relative powers in pin  $n$  at node  $k$  predicted by POLCA and measured by the gamma scans, respectively.  $p_{nk}^c$  and  $p_{nk}^m$  are normalized to the same total assembly power, such that

$$\frac{1}{N * K} \sum_{n=1}^N \sum_{k=1}^K p_{nk}^x = 1 \quad \text{Eq. 5.4}$$

where  $x = c$  or  $m$ ,  $K$  is the number of axial nodes, and  $N$  is the number of fuel rods in the assembly for which measurements were performed.

Statistics involving  $\epsilon$  referred to in this section are defined as follows:

$$RMS_{overall} = 100 * \sqrt{\frac{1}{N * K} \sum_{n=1}^N \sum_{k=1}^K (\epsilon_{nk})^2} \quad \text{Eq. 5.5}$$

$$RMS_{radial} = 100 * \sqrt{\frac{1}{N} \sum_{n=1}^N \left( \frac{1}{K} \sum_{k=1}^K \epsilon_{nk} \right)^2} \quad \text{Eq. 5.6}$$

$$RMS_{axial} = 100 * \sqrt{\frac{1}{K} \sum_{k=1}^K \left( \frac{1}{N} \sum_{n=1}^N \epsilon_{nk} \right)^2} \quad \text{Eq. 5.7}$$

where, as above,  $K$  is the number of axial nodes, and  $N$  is the number of fuel rods in the assembly for which measurements were performed.

The measurement uncertainty in establishing the 1596-keV gamma ray relative intensities is [PROPRIETARY INFORMATION DELETED].

Channel bow perturbs the pin powers but is not included in the POLCA simulation. The effect of channel bow on pin powers depends on the assembly burnup and the radial and axial position at which the local pin power determination is being made. While it is difficult to quantify the effects on pin power uncertainty of channel bow, gamma rays originating from radionuclides other than La-140, and differences between experimental plant conditions and the POLCA simulation, it is important to realize that these effects will impact the agreement between the measured gamma scan results and the POLCA predictions. [PROPRIETARY INFORMATION DELETED].

The SVEA-64 assembly in the Nordic plant for which comparisons were performed is identified as assembly 14779. Assembly 14779 had an average beginning-of-life enrichment of [PROPRIETARY INFORMATION DELETED]. This assembly had [PROPRIETARY INFORMATION DELETED] the measurements were performed. Figure 5.11 shows the pin errors averaged axially for each of the 30 fuel rods for which measurements were performed for this assembly. As shown in Figure 5.11, measurements were performed on 27 UO<sub>2</sub> fuel rods and three UO<sub>2</sub>-Gd<sub>2</sub>O<sub>3</sub> rods.

The agreement between the POLCA predictions and the measured gamma scan results is considered to be quite good. It should be noted that the comparison in Figure 5.11 tests the POLCA capability to predict both nodal power and reconstructed pin powers for a given assembly power. Figure 5.11 also shows a small tilt in the Quadrant Average deviation. This condition is considered to be due to an experimental condition for this measurement that was not captured in the POLCA model. In this case, the most likely experimental condition leading to the mismatch is considered to be channel bow. Nominal inter-assembly gaps were used in the POLCA calculations.

Relative pin powers predicted by POLCA were also compared with fuel rod gamma scan measurements for two SVEA-96 assemblies in a European BWR/6 for which measurements were performed during the outage prior to Cycle 11.

Assembly ADA005 had an assembly average burnup of [PROPRIETARY INFORMATION DELETED] when the measurements were performed. [PROPRIETARY INFORMATION DELETED]. As shown in Figure 5.12, measurements were performed on [PROPRIETARY INFORMATION DELETED].

Figure 5.12 shows the axial average differences between relative pin powers predicted by POLCA and the gamma scan measurements for the 20 rods evaluated from this assembly. The agreement between the POLCA predictions and the measured gamma scan relative pin powers is considered to be quite good. The agreement is excellent for the fuel rod [PROPRIETARY INFORMATION DELETED]. While data are available only for the two northern quadrants for this assembly, there appears to be some tilt in the quadrant average deviation. As for Assembly 14779, the most likely cause of this tilt is considered to be bowing of the channel which is not described in the POLCA predictions.

The gamma scan measurements on assembly ACA001 were performed after the assembly had experienced a burnup of [PROPRIETARY INFORMATION DELETED]. The beginning-of-life average enrichment for this assembly [PROPRIETARY INFORMATION DELETED]. As shown in Figure 5.13, measurements were performed on 28  $\text{UO}_2$  fuel rods and two  $\text{UO}_2\text{-Gd}_2\text{O}_3$ .

Figure 5.13 shows the axial average differences in relative pin errors between the POLCA predictions and the gamma scan measurements for the 30 rods evaluated from this assembly. The agreement between the POLCA predictions and the measured gamma scan results is considered to be very reasonable with a somewhat greater tilt in the differences in powers than for Assemblies 14779 or ADA005. As for Assemblies 14779 and ADA005, the most likely cause of this tilt is considered to be bowing of the channel which is not described in the POLCA predictions. [PROPRIETARY INFORMATION DELETED].

Table 5.5 summarizes the statistics involving the differences in predicted and measured relative pin powers defined by Equations 5.5 through 5.7 for the three assemblies discussed in this section.

As noted above, the nodal pin powers are normalized to the same assembly power. Therefore, with no contribution due to experimental uncertainty,  $\text{RMS}_{\text{overall}}$  would reflect the capability of POLCA to predict relative pin powers in an axial node for a known total assembly power. Similarly,  $\text{RMS}_{\text{radial}}$  would reflect the capability of POLCA to predict the relative rod powers for an assembly with a given power.  $\text{RMS}_{\text{axial}}$  would reflect the capability of POLCA to predict the axial power shape in an assembly with a given power. Since the experimental uncertainties in nodal pin powers are non-zero, the uncertainty in the capability of POLCA to predict nodal pin powers is less than the values shown in Table 5.5. As discussed above, the minimum uncertainty in  $\text{RMS}_{\text{overall}}$  from causes other than the POLCA

calculational capability is **[PROPRIETARY INFORMATION DELETED]**. Therefore, the statistics in Table 5.5 represent conservative estimates of the uncertainties associated with the POLCA capability to predict pin powers. Accordingly, the values in Table 5.5 are averaged over the three assemblies to obtain the following conservative estimates of uncertainties in pin power predicted by POLCA for a given assembly power based on the fuel rod gamma scan results:

**[PROPRIETARY INFORMATION DELETED]**

These estimated uncertainties confirm that the POLCA capability for predicting pin powers is sufficient for the analysis of relevant BWR reactor configurations under steady-state conditions. They indicate that the PHOENIX/POLCA system provides state-of-the-art power predictions acceptable for design and licensing applications.

#### 5.4 CORE REACTIVITY AND POWER DISTRIBUTIONS

Further qualification of the POLCA capability to predict reactivity levels and power distributions is provided in this section. POLCA simulations of operating plant depletions and comparison of POLCA predictions with Traversing In-core Probe (TIP) measurements for three European plants and a plant in the U.S. are presented. In addition, POLCA predictions of nodal and assembly powers are compared with assembly gamma scan measurements performed at two of the plants.

Neutron multiplication factors ( $k_{\text{effective}}$  values) computed by POLCA core follow calculations at hot and cold critical reactor conditions demonstrate the predictability and stability of  $k_{\text{effective}}$  values computed by POLCA. Reactivity comparisons were made at state points for which TIP measurements were performed to provide reasonable confidence that the core was operating under steady-state conditions and that these conditions are well established.

Comparisons of in-core detector responses predicted by POLCA with responses based on TIP measurements provide an indication of the capability of POLCA to provide reliable power distribution predictions. These comparisons are provided for numerous cycle exposures at which TIP measurements were performed for several cycles for each of the four plants evaluated.

Gamma scan measurements for entire assemblies were performed in conjunction with the fuel rod gamma scan measurements discussed in Section 5.3.2. POLCA predictions of the end of cycle (EOC) Ba-140 content were compared with gamma scan measurements of the La-140 activity for a number of assemblies. These gamma scan comparisons provide confirmation of the capability of POLCA to predict assembly nodal and assembly average relative powers. Both the TIP and the gamma scan comparisons reflect the capability of POLCA to accurately predict core power distributions.

Plant A is a Nordic internal pump BWR manufactured by ABB for which fuel rod gamma scan results were compared with POLCA predictions in Section 5.3.2. The Plant A core contains 500 assemblies, and the plant rated power is 2500 MW<sub>th</sub>. Reactivity and TIP comparisons are performed for 18 cycles resulting in a total of 212 hot and 17 cold reactivity comparisons with 212 state points at which TIP comparisons with POLCA predictions are provided. The TIP measurements for these comparisons were obtained with either neutron sensitive or gamma sensitive instruments depending upon the cycle. In addition, assembly powers inferred from gamma scan measurements performed at this plant are compared with POLCA predictions for 26 assemblies after the plant had operated for eight cycles.

Plant B is a European BWR/6 for which fuel rod gamma scan results were compared with POLCA predictions in Section 5.3.2. The Plant B core contains 648 assemblies, and the plant operates with a rated power of 3138 MW<sub>th</sub>. The reactivity and TIP comparisons are provided for 9 cycles resulting in 119 hot and 10 cold reactivity comparisons with 119 state points at which TIP comparisons with POLCA predictions are included. The TIP measurements for these comparisons were performed with gamma sensitive instruments. In addition, assembly powers inferred from gamma scan measurements performed at this plant are compared with POLCA predictions for 47 assemblies after the plant had operated for nine cycles.

Plant C is a modern ABB built BWR for which the measured assembly flow rates were compared with POLCA predictions in Section 5.2. The Plant C core contains 700 assemblies, and the plant operates with a rated power of 3300 MW<sub>th</sub>. The reactivity and TIP comparisons provided in this section are for 12 cycles resulting in 129 hot and 12 cold reactivity comparisons with 129 state points at which TIP comparisons with POLCA predictions are provided. The TIP measurements for these comparisons were performed with either neutron-sensitive or gamma sensitive instruments depending on the cycle.

Plant D is a BWR/4 located in the U.S. Plant D is a C-lattice core containing 764 assemblies, and the plant operates with a rated power of 3293 MW<sub>th</sub>. The reactivity and TIP comparisons are shown for 7.5 cycles resulting in 119 hot and 8 cold reactivity comparisons with 119 state points at which TIP comparisons with POLCA predictions are provided. The TIP measurements for these comparisons were performed with gamma sensitive instruments.

Table 5.6 summarizes the comparisons between measured reactor data and POLCA predictions shown in this section. The number of hot multiplication factor ( $k_{\text{effective}}$ ) state points corresponds to the number of TIP points analyzed since the state points selected for reactivity comparisons are the same as those at which TIP measurements were performed. Similarly, the number of cycles analyzed corresponds to the number of cold measurements performed for Plants A, C, and D since the cold comparisons are only provided at the beginning of each cycle in these cases. Two cold measurements are available for one of the Plant B cycles with a single measurement available for the remaining 8 cycles for this plant.

The term “open lattice” in Table 5.6 refers to fuel rod arrays in which non-boiling water is provided by water rods or water channels which do not include a water cross. The term “SVEA” refers to the ABB design with a water cross attached to the channel walls as described in Reference 22. The SVEA-64 assembly contains four 4x4 subbundles with a water cross. The SVEA-96 and SVEA-96+ designs contain four 24-rod subbundles with a water cross integrated with a central water channel. The SVEA-100 design contains four 5x5, 25-rod subbundles with a water cross.

#### 5.4.1 POLCA Reactivity Predictions

Values for  $k_{\text{effective}}$  calculated at hot conditions at state points for which TIP measurements were performed are provided as a function of cycle burnup in Figures 5.14 through 5.17 for each of the four plants. In addition,  $k_{\text{effective}}$  values calculated at cold conditions at state points for which cold measurements were performed are provided in Figures 5.14 through 5.17.

Consideration of the results in Figures 5.14 through 5.17 is facilitated by understanding how the data are used. ABB performs POLCA core follow calculations for plants for which ABB has nuclear design responsibility or responsibility for licensing analyses requiring POLCA results. Hot and cold reference  $k_{\text{effective}}$  values for use with POLCA are based on these core follow calculations. Historical plant operating data obtained from the utility provide the basis for reference  $k_{\text{effective}}$  values for the initial cycle for which ABB performs licensing analyses, and these reference  $k_{\text{effective}}$  values are updated based on core follow calculations for subsequent cycles. The key factor in this process is sufficiently consistent behavior of the reference  $k_{\text{effective}}$  values to reliably support projections for upcoming cycles. Figures 5.14 through 5.17 demonstrate sufficiently consistent reactivity trends for this purpose.

Specifically, Figures 5.14 through 5.17 show a hot  $k_{\text{effective}}$  trend with burnup which is sufficiently stable from cycle to cycle. The hot  $k_{\text{effective}}$  tends to decrease early in the cycle, become reasonable constant as a function of cycle burnup, and possibly increase toward the end of cycle. The maximum variation within a cycle is typically [PROPRIETARY INFORMATION DELETED]. This predictable, relatively consistent hot  $k_{\text{effective}}$  behavior allows reliable predictions of such design quantities as cycle Full Power Life and Hot Excess reactivity.

The cold  $k_{\text{effective}}$  values show relatively small changes from cycle to cycle with trends in the cold  $k_{\text{effective}}$  occurring over relatively long periods. This behavior allows sufficiently reliable predictions of cold  $k_{\text{effective}}$  values to support, for example, plant startup as well as cold shutdown margin calculations for projected cycles.

Therefore, Figures 5.14 through 5.17 demonstrate that the PHOENIX/POLCA code system with the new cross section library described in Section 2.2, in conjunction with the ABB methodology for establishing reference  $k_{\text{effective}}$  values, provides sufficiently stable and predictable hot and cold reference values of  $k_{\text{effective}}$  to reliably support design and licensing applications.

#### 5.4.2 POLCA Comparisons with TIP Measurements

Traversing In-core Probe (TIP) measurements are compared with detector responses predicted by POLCA in this section. These comparisons provide further confirmation of the capability of POLCA to predict core power distributions.

Comparisons between TIP measurements and POLCA predictions are provided for the same four reactors for which the POLCA reactivity predictions were described in Section 5.4.1. Since measurement uncertainties associated with gamma-sensitive TIP detectors are somewhat lower than the measurement uncertainties associated with neutron-sensitive detectors, it is instructive to understand which detectors were utilized in the comparisons with POLCA. Gamma-sensitive detectors were installed in Plants B and D for all comparisons shown in this section. Neutron-sensitive TIP detectors were utilized in plants A and C until the middle of Cycles 6 and 7, respectively, when gamma-sensitive detectors were installed to replace the neutron-sensitive detectors.

Figures 5.18 through 5.21 present comparisons of the detector responses predicted by POLCA with the TIP measurements for plants A, B, C, and D, respectively. The comparisons are provided in terms of  $RMS_{overall}$  defined by Equation 5.5, where, in this case,  $p_{nk}^c$  and  $p_{nk}^m$  refer to the TIP response predicted by POLCA and the measured TIP response, respectively.  $N$  refers to the number of TIP strings for which comparisons are made. As in Section 5.3.2, the normalization of the predicted and measured TIP responses leads to:

$$\sum_n \sum_k \varepsilon_{nk} = 0 \quad \text{Eq. 5.8}$$

If the measured TIP response is assumed to be known exactly, the  $RMS_{overall}$  defined in this way reflects a measure of the uncertainty in nodal power predicted by POLCA.

Figures 5.22 through 5.25 present comparisons of the detector responses predicted by POLCA with the TIP measurements for plants A, B, C, and D in terms of  $RMS_{Radial}$  defined by Equation 5.6, where  $p_{nk}^c$  and  $p_{nk}^m$ ,  $N$ , and normalization of the measured and predicted TIP responses are defined as described above for  $RMS_{overall}$ . To the extent that the measured TIP response is known exactly,  $RMS_{Radial}$  represents a measure of the uncertainty in assembly power predicted by POLCA.

As shown in Figures 5.18, 5.20, 5.22, and 5.24, the improvement in the quality of the measured signal associated with gamma-sensitive TIPs is clearly indicated by the decreases in RMS values in Cycles 6 for Plant A and Cycle 7 for Plant C.

As for the comparisons between gamma scan measurements and POLCA predictions in Section 5.3.2, no attempt has been made to correct the comparisons in Figures 5.22 through 5.25 for measurement uncertainties.

Table 5.7 summarizes values of  $RMS_{overall}$  and  $RMS_{radial}$  based on the average measured and predicted TIP responses over all cycles for each of the four plants. Since lower measurement uncertainties are associated with the measurements obtained with the gamma-sensitive TIPs, the averages for Plants A and C were taken only over those points for which the measurements were obtained with the gamma-sensitive TIPs. This approach provides an improved estimate of the uncertainty associated with the POLCA calculations since the measurement uncertainty is reduced. The average  $RMS_{overall}$  and average  $RMS_{radial}$  values in Table 5.7 averaged over all four plants are 4.3% and 1.5%, respectively.

The RMS values shown in Figures 5.18 through 5.25 and Table 5.7 confirm the capability of POLCA to reliably predict nodal powers and assembly powers. Since no attempt has been made to subtract experimental uncertainties associated with the TIP measurements, the RMS values in Table 5.7 are judged to represent conservative estimates of the POLCA uncertainty in nodal and assembly power. Furthermore, Figures 5.18 through 5.25 do not indicate significant trends or biases in the RMS values based on TIP results obtained with gamma-sensitive instruments over several cycles. Therefore, the averages in Table 5.7 are considered to be a good representation of the agreement which can be expected between POLCA predictions and TIP measurements in general.

#### 5.4.3 Nodal Gamma Scans

This section contains comparisons of assembly nodal and relative assembly average BA-140 concentrations predicted by POLCA with gamma scan measurements performed on fuel assemblies in the same two plants for which the relative fuel pin power comparisons are provided in Section 5.3.2. As discussed in Section 5.3.2, comparisons between Ba-140 concentrations and measured La-140 activities provide an indication of the capability of POLCA to predict relative power distributions. These plants are referred to as Plants A and B in Section 5.3.2. As explained in Section 5.3.2, Plant A is a Nordic BWR, and Plant B is a European BWR/6. Information regarding these plants and the fuel types composing the cores is included in Table 5.6. These comparisons of gamma scan results with POLCA predictions provide further qualification of the capability of POLCA to predict assembly nodal and relative assembly powers.

The assembly gamma scan measurements are performed using the same technique used for the fuel rod gamma scan measurements discussed in Section 5.3.2. The relative intensities of the 1596-keV gamma rays from the decay of La-140 are measured at assembly axial locations which can be related to POLCA nodes. For the assembly measurements, the activity at a given axial position is based on measurements at the four corners of the assembly.

As in the case of the fuel rod gamma scan measurements, the measurement uncertainty in establishing the 1596-keV gamma ray relative intensities at a given axial location is [PROPRIETARY INFORMATION DELETED]. As in Section 5.3.2, the [PROPRIETARY INFORMATION DELETED] of all the contributions to the uncertainties which are not associated with the POLCA capability to predict nodal powers. The same effects identified in Section 5.3.2 for the fuel pin comparisons which contribute to the uncertainty in the comparison between POLCA predictions and the measurements which are not accounted for in the [PROPRIETARY INFORMATION DELETED] and are not associated with the POLCA calculational capability are also present in the fuel assembly comparisons to gamma scan measurements. As noted in Section 5.3.2, these contributions are due to [PROPRIETARY INFORMATION DELETED]. Nevertheless, it should be recognized that  $\epsilon_{nk}$  (defined in Section 5.3.2) and statistics based on  $\epsilon_{nk}$  without any correction due to experimental uncertainties and the additional effects noted above represent an over estimate of the uncertainty associated with the POLCA calculation.

The fuel assembly gamma scan measurements were performed at Plant A during the annual shutdown which occurred after 8 cycles of operation. Measurements were performed for a total of 26 fuel assemblies with [PROPRIETARY INFORMATION DELETED]. These measurements were performed on 14 SVEA-64 assemblies and 12 open-lattice 8x8-2 assemblies.

The fuel assembly gamma scan measurements at Plant B were performed for a total of 47 fuel assemblies with [PROPRIETARY INFORMATION DELETED]. The population of 47 assemblies is composed of 16 SVEA-96, 16 8x8-2 open lattice assemblies, and 15 8x8-4 assemblies with a central water channel.

In the discussion below, the quantities  $\epsilon_{nk}$ ,  $p_{nk}^x$ ,  $RMS_{overall}$ ,  $RMS_{radial}$ , and  $RMS_{axial}$  have the same definitions provided in Section 5.3.2 where, in this case:

$p_{nk}^x$  = relative value corresponding to a POLCA node with  $x = c$  (Ba-140 concentration calculated by POLCA) or  $m$  (La-140 activity from the gamma scan measurements), and

$N$  = the number of assemblies in the population over which the  $p_{nk}^x$  are normalized and  $RMS_{overall}$ ,  $RMS_{radial}$ , and  $RMS_{axial}$  are calculated.

The "Assembly Average Difference" referred to in this section is defined as:

$$AssemblyAverageDifference = \frac{100}{K} \sum_{k=1}^K \epsilon_{nk} \quad Eq. 5.9$$

This parameter reflects relative assembly power within the population over which the  $p_{nk}^x$  are normalized.

Figure 5.26 shows the Assembly Average Differences for the 26 assemblies for which gamma scan measurements were performed at Plant A. The population over which the  $p_{nk}^x$  are normalized, and for which the global statistics discussed below are established, in this case is the entire set of 26 assemblies including the SVEA-64 and 8x8-2 assembly types. This approach is justified by the fact that the two assembly types had reasonably similar average burnups and the designs themselves are sufficiently similar. Specifically, the average burnups of the SVEA-64 and 8x8-2 assemblies were [PROPRIETARY INFORMATION DELETED], respectively. While the assemblies differ in design due to the presence of a water cross in the SVEA-64 design, both assemblies have the same number of fuel rods, and the fuel rods have similar diameters.

The agreement between the measurements and calculations in Figure 5.26 is considered to be very good. Inspection of the results show no clear biases or trends with respect to fuel type (SVEA-64 or 8x8-2 open lattice) or core position. It is noteworthy that the relative assembly power predictions are in good agreement with the experimental data on the core periphery and in the partially controlled assemblies. Assemblies 17,18 and 10,9 in Figure 5.26 were adjacent to a control rod which was withdrawn to about node 7.

Figures 5.27 through 5.29 show the Assembly Average Differences for the 47 assemblies for which gamma scan measurements were performed at Plant B. In this case, the SVEA-96, 8x8-2 and 8x8-4 assembly designs and average burnups are considered to be sufficiently dissimilar to require that each assembly type be considered a separate population. Accordingly, the three populations for which the  $p_{nk}^x$  are normalized and the global statistics discussed below are established are shown in Table 5.8:

The agreement between the measurements and calculations in Figures 5.27 through 5.29 is considered to be very good. Inspection of the results show no clear biases or trends with respect to fuel type (SVEA-96, 8X8-2 Open Lattice, or 8x8-4 with single central water channel assemblies) or core position. The spread in the results appears to be somewhat greater for the 8x8 assemblies than for the SVEA-96 assemblies. It is judged that this slightly greater spread in Assembly Average Differences may be due to the higher average assembly burnups of the 8x8 assemblies which typically leads to a greater spread in channel bow. As discussed above, the measured data have not been corrected for the effects of channel bow.

Table 5.9 summarizes the global statistics described above for Plants A and B. The averages of Plant A and B results in Table 5.9 represent an overall comparison of the POLCA predictions with the gamma scan results. The results in Table 5.9 have not been corrected for the uncertainty in the La-140 activity measurements or the other effects not associated with the capability of POLCA to predict assembly and nodal powers which lead to differences between the POLCA predictions and the gamma scan measurements. Consequently, the statistics in Table 5.9 provide a conservative estimate, or an over estimate, of the uncertainty due to POLCA calculational capability. Therefore,  $RMS_{overall}$  represents a conservative estimate of the relative uncertainty in nodal power calculated by POLCA for a given core power.  $RMS_{radial}$  represents an estimate of the relative uncertainty in assembly power calculated by POLCA for a given core power. Comparison of the three RMS statistics in Table 5.9 indicates that the major component of  $RMS_{overall}$  is due to differences in POLCA axial power shape predictions and the measurements. A partial contribution to this situation which is not related to the POLCA predictions is the effect of channel bow which varies with axial position. The hypothesis that channel bow is affecting the results in the Plant B statistics is also consistent with the higher 8x8-type assembly RMS values relative to those for SVEA-96 since the 8x8-type assemblies had somewhat higher burnups than the SVEA-96 assemblies.

It is concluded that the comparisons of POLCA predictions with the TIP measurements in Section 5.4.2 and the gamma scan measurements in this section confirm that the POLCA capability for predicting nodal and assembly powers is sufficient for the analysis of relevant BWR reactor configurations under steady-state conditions. These comparisons also confirm that the PHOENIX/POLCA system provides state-of-the-art nodal and assembly power predictions which are acceptable for design and licensing applications.

## 5.5 PERFORMANCE RELATIVE TO CURRENT PHOENIX/POLCA SYSTEM

As discussed in Section 1, the PHOENIX/POLCA code system described in this topical report is an improved version of the system discussed in Reference 1. Relative to the PHOENIX/POLCA code system described in Reference 1, the version described herein is based on a new cross section library and incorporates improvements in the POLCA calculational models. The improvements incorporated into POLCA are summarized in Section 1.2 and discussed in Section 4.

The PHOENIX/POLCA version described in Reference 1 has been accepted for referencing in licensing applications and is, therefore, currently used for licensing analyses. Consequently, it is informative to compare the improved code version described in this report with the version discussed in Reference 1. The comparison is provided in this section in the form of hot and cold reactivity predictions and comparisons with TIP measurements for the two code systems. Results based on the current code system discussed in Reference 1 are referred to as "Current", and results based on the code system discussed in this report are referred to as "New". References to "POLCA" or "PHOENIX/POLCA" in other sections of this report refer, of course, to the New code system. The comparisons are provided for Plants A, B, and C, where the characteristics of Plants A, B, and C are discussed in Sections 5.3.2 and 5.4.

### 5.5.1 Reactivity Comparisons

The hot and cold  $k_{\text{effective}}$  values computed with the Current and New code systems are plotted in Figures 5.30 through 5.32 for Plants A, B, and C, respectively. The  $k_{\text{effective}}$  results for the New code system are the same as those shown in Figures 5.14 through 5.16. Inspection of Figures 5.30 through 5.32 confirms that both the Current and New code systems, in conjunction with the ABB methodology for establishing reference  $k_{\text{effective}}$  values, provide sufficiently stable and predictable hot and cold reference values of  $k_{\text{effective}}$  to reliably support design and licensing applications. However, reactivity predictions with the New code system represents an improvement relative to the Current code system for the following reasons:

1. Hot  $k_{\text{effective}}$  values calculated with the New code system generally show less variation from cycle-to-cycle and a smaller variation within the each cycle than those calculated with the Current code system. Therefore, projections of upcoming cycle hot reactivities are expected to be more reliable with the New code system.

2. Variations in the cold  $k_{\text{effective}}$  values calculated with the New code system generally show somewhat less variation from cycle to cycle than those calculated with the Current Code system. Therefore, projections of upcoming cycle cold reactivities are expected to be more reliable with the New code system.
3. Differences in magnitude between calculated hot and cold  $k_{\text{effective}}$  values are substantially reduced with the New code system. Furthermore, calculated hot reactivities are substantially closer to unity with the New version of POLCA. Since the ABB methodology utilizes reference hot and cold values of  $k_{\text{effective}}$  based on core follow data, proximity of the hot and cold values to each other or to unity is not required. However, closer proximity of predicted reactivities to unity, and of hot and cold  $k_{\text{effective}}$  to each other indicate an improved absolute prediction of physical reality.

### 5.5.2 TIP Comparisons

Comparisons between POLCA predictions and TIP measurements computed with the Current and New code systems are plotted in Figures 5.33 through 5.38 for Plants A, B, and C, respectively. Values of  $\text{RMS}_{\text{overall}}$  and  $\text{RMS}_{\text{radial}}$  defined in Section 5.4.2 are shown in Figures 5.33 through 5.35 and Figures 5.36 through 5.38, respectively, over several cycles of operation. The RMS values for the New code system are the same as those shown in Figures 5.18 through 5.20 and Figures 5.22 through 5.24.

Figures 5.33 through 5.38 confirm that the Current and New code systems provide sufficient agreement with measured TIP data to reliably support design and licensing applications. However, the agreement with the TIP data for the New code system represents an improvement relative to the Current code system. Both the  $\text{RMS}_{\text{overall}}$  values, which reflect the capability of POLCA to predict relative nodal powers, and the  $\text{RMS}_{\text{radial}}$  values, which reflect the capability of POLCA to predict relative assembly powers, are generally reduced for the New code system relative to the Current code system.

**Tables 5.1 through 5.9**

**[PROPRIETARY INFORMATION DELETED]**

**Figures 5.1 through 5.7**

**[PROPRIETARY INFORMATION DELETED]**

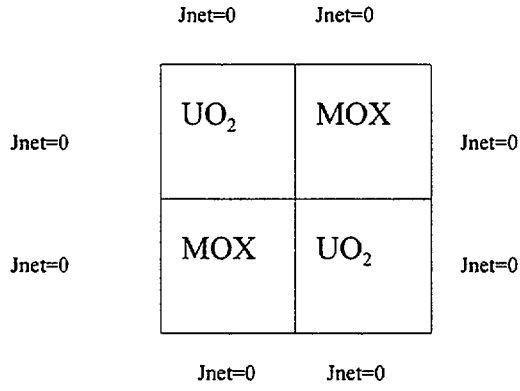


Figure 5.8: UO<sub>2</sub>/MOX Checkerboard for NEACRP-L336 Benchmark

**Figures 5.9 through 5.38**

**[PROPRIETARY INFORMATION DELETED]**

## 6.0 SUMMARY

The PHOENIX/POLCA code system has been used for the analysis of Nordic reactors since the late 1960's. This code system, as described in Reference 1, has been used in the United States since the mid 1980's. In addition, the POLCA 3D core simulator has been used for on-line core monitoring in Nordic plants since 1974.

The PHOENIX/POLCA code system described in this topical report is an improved version of the system discussed in Reference 1. Relative to the PHOENIX/POLCA code system described in Reference 1, the version described herein is based on a new cross section library and incorporates improvements in the POLCA calculational models. The new library and the improvements in POLCA are described in Sections 2 and 4.

The new PHOENIX/POLCA code system with the new cross section library has been tested by comparison with higher order analytical solutions and experimental data. Code predictions have been compared with critical facility measurements as well as operating plant data. This section summarizes results and conclusions based on the qualification relative to measurements discussed in Sections 3 and 5 as well as overall conclusions.

### 6.1 PHOENIX BENCHMARKS TO TEST THE NEW LIBRARY

The calculational models, approximations and methods in the PHOENIX code are the same as those described in Reference 1. Qualification results with the new 34-group cross section library are provided in Section 3 as an illustration of the ABB methodology for qualifying a new cross section library. PHOENIX, and the associated nuclear data pre- and post-processing codes, has been modified only to the extent required to support the new cross section library and the POLCA improvements.

Since the primary application of PHOENIX is to generate the few-group nodal cross sections and other physics constants for POLCA, the best overall qualification of PHOENIX and the new library is the comparison of POLCA predictions with experimental data described in Chapter 5. However, comparison of PHOENIX predictions with measured data allows the capability of PHOENIX, in conjunction with the new 34-group cross section library, to be evaluated independent of approximations involved in the POLCA methods and the additional experimental uncertainties involved with operating plant measurements. The comparisons with the Strawbridge and Barry and BAPL uniform lattice critical measurements confirmed the

capability of PHOENIX to accurately calculate reactivity over a wide range of lattice parameters. Because of the simple geometry in those experiments, the comparisons primarily provided verification and validation of the new cross section library.

In addition, the ability of PHOENIX to accurately predict bundle reactivity and internal (local) power distributions was verified by comparison with experimental results obtained for nonuniform  $\text{UO}_2$  and  $\text{PuO}_2$  lattices performed at the KRITZ critical facility.

As shown in Table 3.10, the mean  $k_{\text{effective}}$  for the  $\text{UO}_2$  Strawbridge and Barry criticals, the BAPL criticals, and the  $\text{UO}_2$  and  $\text{PuO}_2$  KRITZ experiments is [PROPRIETARY INFORMATION DELETED] with a total spread in the average  $k_{\text{effective}}$  values for each of the four experimental sets of [PROPRIETARY INFORMATION DELETED]. The proximity to unity and the relatively small spread in these average values demonstrate excellent agreement with the experimental data.

Furthermore, the PHOENIX predictions showed very good agreement with the KRITZ pin power (i.e. fission rate) measurements. The mean absolute differences in predicted and measured pin powers were [PROPRIETARY INFORMATION DELETED] for the  $\text{UO}_2$  and  $\text{PuO}_2$  KRITZ experiments, respectively, with corresponding maximum differences of [PROPRIETARY INFORMATION DELETED].

The combination of these results confirm that PHOENIX, in conjunction with the new ENDF/B-VI based 34-group library, provides state-of-the-art reactivity and relative pin power predictions for a broad range of conditions and temperatures.

## 6.2 POLCA Qualification

The qualification of POLCA in Section 5 is divided into two categories, referred to as verification and validation. In the context of this report, verification involves the testing of individual models or combinations of models to verify that they perform as intended. Validation involves the comparison of POLCA predictions with measured data to establish the accuracy of the system operating as a whole. The POLCA verification was performed by comparison with computational benchmarks generated by means of reference calculations as well as by comparison with experimental data suitable for evaluating the individual model being verified. The POLCA validation involved the evaluation of core follow predictions for four reactors as well as comparisons with gamma scan measurements performed at two of the reactors.

## 6.2.1 Reactivity

ABB performs POLCA core follow calculations for plants for which ABB has nuclear design responsibility or responsibility for licensing analyses requiring the POLCA results. Hot and cold reference  $k_{\text{effective}}$  values for use with POLCA are based on these core follow calculations. The key factor in this process is to obtain sufficiently consistent behavior of the reference  $k_{\text{effective}}$  values to reliably support projections for upcoming cycles.

Hot and cold  $k_{\text{effective}}$  values based on core follow calculations over numerous cycles for four plants are shown in Section 5.4.1. The results in Section 5.4.1 demonstrate that hot  $k_{\text{effective}}$  values show a predictable and relatively small variation [PROPRIETARY INFORMATION DELETED] within successive cycles. Furthermore, hot and cold  $k_{\text{effective}}$  values show relatively small changes from cycle to cycle with trends developing fairly gradually over relatively long periods. Therefore, it is concluded that the PHOENIX/POLCA code system with the new cross section library provides sufficiently stable and predictable hot and cold reference values of  $k_{\text{effective}}$  to reliably support design and licensing applications.

## 6.2.2 Power Distributions

The capability of POLCA to predict relative nodal pin, fuel rod, nodal average, and assembly power distributions is evaluated in Section 5 by comparisons with TIP data and gamma scan measurements. The TIP measurements are based on core follow calculations over numerous cycles for four plants as discussed in Section 5.4. Comparisons of POLCA predictions with the TIP readings and the fuel assembly gamma scan measurements provide an indication of the relative nodal and assembly power uncertainties associated with POLCA. Comparisons of POLCA predictions with the fuel rod gamma scan measurements provide an indication of the relative nodal pin power and fuel rod power uncertainties associated with POLCA.

### 6.2.2.1 Relative Nodal Pin and Fuel Rod Power Uncertainties

The capability of POLCA to predict relative nodal pin and fuel rod powers was evaluated by comparing POLCA predictions with the results of fuel rod gamma scan measurements performed on three ABB BWR assemblies in two European reactors. The evaluation in Section 5.3.2 is based on gamma scan measurements performed on a total of 30 SVEA-64 fuel rods after operation in one of the reactors and 50 SVEA-96 fuel rods after operation in the second reactor. The following conservative estimates of uncertainties in pin powers predicted by POLCA for a given fuel assembly power are based on the evaluations presented in Section 5.3.2:

| [PROPRIETARY INFORMATION DELETED]

These uncertainties are expressed in terms of the Root Mean Square (RMS) values defined in Section 5.3.2. They are considered to be conservative since they have not been corrected for experimental uncertainty.

These estimated uncertainties confirm that the POLCA capability for predicting pin powers is sufficient for the analysis of relevant BWR reactor configurations under steady-state conditions.

#### 6.2.2.2 Relative Nodal and Assembly Average Power Uncertainties

The capability of POLCA to predict relative nodal and assembly average powers was evaluated by comparing POLCA predictions with the results of assembly gamma scan measurements performed at the same two European reactors at which the fuel rod gamma scan measurements were performed, as well as TIP measurements at three European plants and a U.S. plant over numerous cycles. The evaluation in Section 5.4 is based on gamma scan measurements performed on a total of 26 fuel assemblies in one plant and 47 fuel assemblies in the second plant. The comparisons with gamma-sensitive TIP measurements in the four plants were performed for over 33.5 cycles.

The following estimates of uncertainties in nodal, assembly, and axial power shape predicted by POLCA are based on the evaluation of assembly gamma scan data in Section 5.4.3:

| [PROPRIETARY INFORMATION DELETED]

These uncertainties are expressed in terms of the RMS values discussed in Section 5.4.3. They are considered to be conservative since they have not been corrected for experimental uncertainty.

The comparisons between POLCA predictions and TIP results obtained with gamma-sensitive detectors show very good agreement with the results based on gamma scan measurements quoted above. For example, the RMS values based on comparisons of POLCA results with the TIP measurements averaged over all four plants corresponding to the Relative Nodal Power and Relative Assembly Power uncertainties quoted above are [PROPRIETARY INFORMATION DELETED] respectively.

This agreement between POLCA predictions and gamma scan as well as TIP measurements is considered to be very good. In addition to the relatively small uncertainties observed, the results show no clear biases or trends with respect to fuel type or core position. It is concluded that the comparisons of POLCA predictions with the TIP and assembly gamma scan measurements confirm that the POLCA capability for predicting nodal and assembly powers is sufficient for the analysis of relevant BWR reactor configurations under steady-state conditions.

### 6.2.3 Pressure Drops and Relative Assembly Flow

The thermal-hydraulic model in POLCA is an updated version of the model contained in the original version of POLCA described in Reference 1. Therefore, the qualification measures discussed in Reference 20 and supporting Reference 1 also provide verification of the new POLCA version discussed in this report. In addition, benchmarking of the hydraulic model in POLCA has been expanded in this document by comparing POLCA predictions with test loop data and in-core measurements. Specifically, comparisons of POLCA predictions with FRIGG Loop two-phase pressure drop measurements and assembly flows measured in an ABB Nordic reactor are provided in Section 5.2.

The agreement between the FRIGG Loop pressure drop measurements and POLCA predictions discussed in Section 5.2 provides general confirmation that the thermal-hydraulic models in POLCA are capable of accurately predicting local and overall pressure drops in a typical BWR assembly. Furthermore, comparison of measured and predicted channel flows resulted in an overall Root Mean Square Error of **[PROPRIETARY INFORMATION DELETED]** indicating that POLCA is predicting relative assembly flows with a high degree of accuracy. Therefore, these results provide further confirmation that the models in POLCA are providing an accurate simulation of the hydraulic performance of a BWR core.

### 6.3 OVERALL CONCLUSION

The qualifications of the PHOENIX/POLCA code system are based on comparisons with higher order calculations, measurements from operating BWRs, and experimental results from critical configurations. These comparisons demonstrate that the methodology is capable of satisfactory analysis of relevant BWR reactor configurations and steady-state operating conditions. Comparisons with the Current version of the PHOENIX/POLCA code system documented in Reference 1 demonstrate that the agreement between code predictions and measurements is improved relative to the accepted methods. Furthermore, the qualification comparisons have covered a reasonable range of parameters, conditions, higher order calculations and available experimental data.

Therefore, it is concluded that the qualification process has demonstrated the PHOENIX/POLCA capability analysis of relevant BWR reactor configurations under steady-state conditions. The PHOENIX/POLCA system provides state-of-the-art results acceptable for design and licensing applications.

## 7.0 REFERENCES

1. ABB Atom Nuclear Design and Analysis Programs for Boiling Water Reactors: Programs Description and Qualification, BR 91-402-P-A (proprietary), BR 91-403-NP-A (nonproprietary), May 1991.
2. A Description of the Nuclear Design and Analysis Programs for Boiling Water Reactors, Westinghouse Report WCAP-10106-P-A (proprietary), WCAP-10999-NP-A (nonproprietary), September 1985.
3. Qualification of the PHOENIX/POLCA Nuclear Design and Analysis Programs for Boiling Water Reactors, Westinghouse Report WCAP-10841-P-A (proprietary), WCAP-10842-NP-A (nonproprietary), June 1985.
4. Letter from C. O. Thomas (NRC) to E. P. Rahe (W), "Acceptance for Referencing of Licensing Topical Report WCAP-10106, 'A Description of the Nuclear Design and Analysis Programs for Boiling Water Reactors'," September 3, 1985.
5. Letter from M. W. Hodges (NRC) to W. J. Johnson (W), "Acceptance for Referencing of Licensing Topical Report WCAP-10841, 'Qualification of the PHOENIX/POLCA Nuclear Design and Analysis Programs for Boiling Water Reactors'," June 14, 1988.
6. Letter from A. L. Thadani (NRC) to J. Lindner (ABB Atom), "Designation of ABB Atom Topical Reports Related to Licensing of ABB Atom Reload Fuel," June 18, 1992.
7. Letter from G. Heimersson (ABB Atom) and A. E. Scherer (ABB CE) to R. C. Jones, Jr. (NRC), "ABB BWR Fuel and Core Component Licensing Activities," September 4, 1992.
8. P. F. Rose and C. L. Dunford, Eds., "ENDF-102, Data Formats and Procedures for the Evaluated Nuclear Data File, ENDF-6," Brookhaven National Laboratory, Report BNL-NCS-44945, July 1990 and Revisions October 1991, November 1995 and February 1997.
9. R. E. MacFarlane, D. W. Muir, "The NJOY Nuclear Data Processing System Version 1," LA-12740-M, October 1994.
10. B. Fredin, U. Decher, A. Jonsson, A. Ferri and R. J. J. Stammeler, "Processing and Application of ENDF/B-VI in LWRs: Critical Experiments," *Trans. Am. Nucl. Soc.*, Vol. 73, p. 419, 1995.
11. American National Standard, Nuclear Data Sets for Reactor Design Calculations, ANSI/ANS-19.1-1983.

12. P. Kier, A. Robba, "RABBLE, A Program for Computation of Resonance Absorbption in Multi-Region Reactor Cells," ANO-7326, 1967.
13. U. Decher, A. Jonsson, S. J. Kim and K. S. Kim, "ENDF/B-VI Performance in PWR Applications," *Trans. Am. Nucl. Soc.*, Vol. 73, p. 417, 1995.
14. L. E. Strawbridge, R. F. Barry, "Criticality Calculations for Uniform Water-Moderated Lattices," *Nucl. Sci. Eng.*, Vol. 23, 1965.
15. CSEWG "Benchmark Specifications," Brookhaven National Laboratory, ENDF-2-2, BNL 19302, November 1981.
16. R. Persson, E. Blomsjo, M. Edenius, "High Temperature Critical Experiments with H<sub>2</sub>O Moderated Fuel Assemblies in KRITZ," In *Technical Meeting No. 2/11, Nucllex72*, 1972.
17. K. S. Smith, "An Analytic Nodal Method for Solving the Two-Group Multidimensional, Static and Transient Neutron Diffusion Equation," Department of Nuclear Engineering Thesis, M.I.T., Cambridge, Mass., March 1979.
18. F. Bennewitz et al., "Solution of the Multidimensional Neutron Diffusion Equation by Nodal Expansion," CONF-750413, Proc. Conf. on Comput. Methods in Nucl. Eng., Vol .1 p. 99, Charleston, South Carolina, 1975.
19. D. L. Vogel and Z. J. Weiss, "A General Multigroup Formulation of the Analytic Nodal Method," Proc. Top. Mtg. Advances in Reactor Physics, Charleston, South Carolina, March 1992.
20. CONDOR: A Thermal-Hydraulic Performance Code for Boiling Water Reactors, BR 91-255-P-A Rev. 1 (proprietary), BR 91-255-NP-A Rev. 0 (nonproprietary), May 1991.
21. L. Haar, J. S. Gallagher, G. S. Kell, "NBS/NRC Steam Tables: Thermodynamic and Transport Properties and Computer Program for Vapor and Liquid States of Water in SI Units," Hemisphere Publishing Corporation, London, 1984.
22. Reference Safety Report for Boiling Water Reactor Reload Fuel, CENPD-300-P-A (proprietary), CENPD-300-NP-A (nonproprietary), July 1996.

23. SVEA-96 Critical Power Experiments on a Full-Scale 24-Rod Sub-Bundle, UR 89-210-P-A (proprietary), UR 89-210-NP-A (nonproprietary), October 1993.
24. 10x10 SVEA Fuel Critical Power Experiments and CPR Correlations: SVEA-96+, CENPD-389-P, June 1998.
25. R. R. Lee et al., "The Benchmark Problem Book," Argonne Code Centre, Report ANL-7416, Supplement 2, 1977.
26. E. Z. Muller and Z. J. Weiss, "Benchmarking with the Multigroup Diffusion High-Order Response Matrix Method," *Annals of Nuclear Energy*, Vol. 18, No. 9, p. 534, 1991.
27. K. S. Smith, "Assembly Homogenization Techniques for Light Water Reactor Analysis," *Progress in Nuclear Energy*, Vol. 17, No. 3, pp. 303-335, 1986.
28. E. Z. Muller et al., "Development of a Core Follow Computational System for Research Reactors," Ninth Pacific Basin Nuclear Conference, Sydney, Australia, May 1994.
29. K. Koebke et al., "The Benchmark Problem Book," Argonne Code Centre, Report ANL-7416, Supplement 3, 1985.
30. J. Lefvebre, J. Mondot and J. P. West, "Benchmark Calculations of Power Distribution Within Assemblies (Specification)," NEACRP-L-336, 1991.

*Intentionally Left Blank*

**APPENDIX A [PROPRIETARY INFORMATION DELETED]**

**APPENDIX B [PROPRIETARY INFORMATION DELETED]**

**APPENDIX C [PROPRIETARY INFORMATION DELETED]**

**APPENDIX D [PROPRIETARY INFORMATION DELETED]**

# **ABB Combustion Engineering Nuclear Power, Inc.**

ABB Combustion Engineering Nuclear Power, Inc.  
2000 Day Hill Road  
Post Office Box 500  
Windsor, Connecticut 06095-0500